Molecular Therapy
Original Article

Cut and Paste: Efficient Homology-Directed Repair of a Dominant Negative *KRT14* Mutation via CRISPR/Cas9 Nickases

Thomas Kocher,[1] Patricia Peking,[1] Alfred Klausegger,[1] Eva Maria Murauer,[1] Josefina Piñón Hofbauer,[1] Verena Wally,[1] Thomas Lettner,[1] Stefan Hainzl,[1] Michael Ablinger,[1] Johann Wolfgang Bauer,[2] Julia Reichelt,[1] and Ulrich Koller[1]

[1]EB House Austria, Research Program for Molecular Therapy of Genodermatoses, Department of Dermatology, University Hospital of the Paracelsus Medical University Salzburg, 5020 Salzburg, Austria; [2]Department of Dermatology, University Hospital of the Paracelsus Medical University Salzburg, 5020 Salzburg, Austria

With the ability to induce rapid and efficient repair of disease-causing mutations, CRISPR/Cas9 technology is ideally suited for gene therapy approaches for recessively and dominantly inherited monogenic disorders. In this study, we have corrected a causal hotspot mutation in exon 6 of the keratin 14 gene (*KRT14*) that results in generalized severe epidermolysis bullosa simplex (EBS-gen sev), using a double-nicking strategy targeting intron 7, followed by homology-directed repair (HDR). Co-delivery into EBS keratinocytes of a Cas9 D10A nickase (Cas9n), a predicted single guide RNA pair specific for intron 7, and a minicircle donor vector harboring the homology donor template resulted in a recombination efficiency of >30% and correction of the mutant *KRT14* allele. Phenotypic correction of EBS-gen sev keratinocytes was demonstrated by immunofluorescence analysis, revealing the absence of disease-associated K14 aggregates within the cytoplasm. We achieved a promising safety profile for the CRISPR/Cas9 double-nicking approach, with no detectable off-target activity for a set of predicted off-target genes as confirmed by next generation sequencing. In conclusion, we demonstrate a highly efficient and specific gene-editing approach for *KRT14*, offering a causal treatment option for EBS.

INTRODUCTION

The CRISPR/Cas9 genome-editing technology is capable of modifying genes in a precise and efficient manner, and has become a widely used tool in medical research for the correction of disease-associated mutations. The rescue of a disease phenotype by specific correction of a mutation is executed via a cut-and-paste strategy. Modified from a naturally occurring bacterial defense mechanism, the Cas9 nuclease induces DNA double-strand breaks (DSBs), which activate the cell's endogenous repair machinery, thus offering the possibility for genetic modifications. The specificity of the CRISPR/Cas9 technology is determined by a single guide RNA (sgRNA), which is designed to be complementary to the targeted genomic region and linked to the Cas9 nuclease, ensuring specifically targeted DSB induction (Figure 1A). Subsequently, cells repair such DSBs either by non-homologous end joining (NHEJ), wherein the DNA ends are randomly ligated, thereby introducing small insertions or deletions, or by homology-directed repair (HDR), where endogenously or externally supplied homologous donor templates are incorporated into the DNA at the site of the DSB.[1] Exploiting this technology, genomic sequences can be extensively modified, allowing the introduction or knockout of genes, the creation of distinct deletions or insertions, or the specific correction of any disease-associated mutation.[2–4]

Nevertheless, the likelihood of off-target effects, as seen when using the wild-type CRISPR/Cas9 system derived from streptococcus pyogenes (spCas9), remains an important issue to be addressed. One way to improve the targeting specificity, and to further shift the preferred repair mechanism from the unspecific NHEJ to the more specific HDR, is to utilize two distinct sgRNAs in combination with a modified Cas9 nuclease (Cas9 D10A nickase [Cas9n]), which, by virtue of its mutated RuvC nuclease domain, instead causes paired nicks, one on each strand of the target sequence, which is tantamount to inducing a DSB at the desired gene locus (Figure 1A). Recently, Ran et al.[5] successfully performed double-nicking-mediated gene targeting with an efficient offset distance of up to 100 bp between the protospacer adjacent motif (PAM)-distal (5′) ends of both sgRNA sequences, which revealed a significant decrease of off-target activity compared with the spCas9, because of the fact that potential off-target single nicks are more likely to be repaired without causing deletions or insertions.[5–7] The chance of unspecific binding of both sgRNAs in close proximity to each other at any location other than the desired locus, and thereby inducing a DSB, is unlikely, which can be confirmed via next generation sequencing (NGS) of potential off-target regions. It is an essential pre-clinical requirement for any specific CRISPR/Cas9 molecule to ensure high on-target activity in combination with negligible off-target activity.

Received 18 May 2017; accepted 17 August 2017;
http://dx.doi.org/10.1016/j.ymthe.2017.08.015.

Correspondence: Ulrich Koller, EB House Austria, Department of Dermatology, University Hospital of the Paracelsus Medical University Salzburg, Strubergasse 22, 5020 Salzburg, Austria.
E-mail: u.koller@salk.at

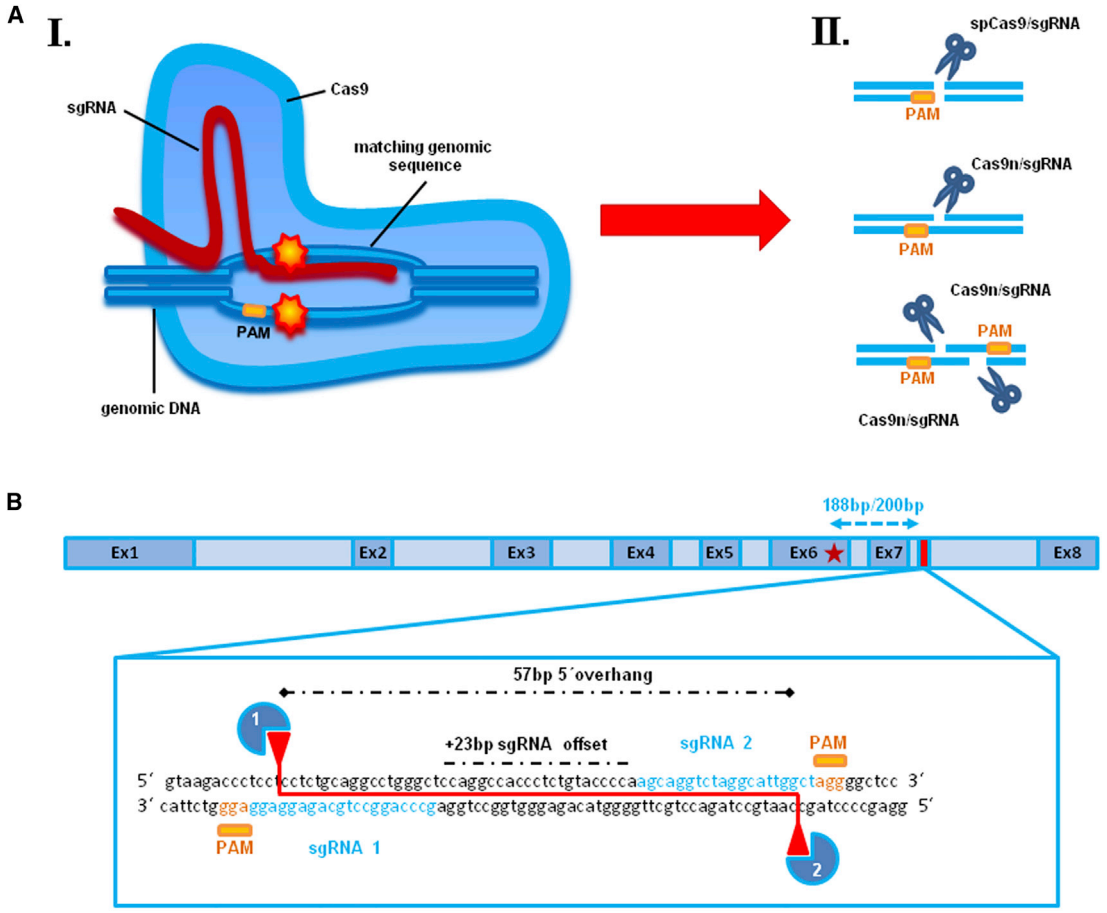

Figure 1. CRISPR/Cas9 Technology: Design of sgRNA Pair for Double-Nicking within *KRT14* Intron 7

(A) Schematic depiction of the CRISPR/Cas9 mechanism. (AI) The specificity of the CRISPR/Cas9 technology is determined by a single guide RNA (sgRNA), which is designed to be complementary to the targeted genomic region and linked to the Cas9 nuclease, ensuring specific and directed genomic DSB induction. Such DSBs are repaired by cellular mechanisms such as non-homologous end joining (NHEJ) or homology-directed repair (HDR), where endogenously or externally supplied homologous donor sequences are specifically incorporated into the DNA at the site of the DSB. (II) Cas9 nuclease induces DNA double-strand breaks (DSBs), which activate the cell's endogenous repair machinery. A modified Cas9 nuclease (Cas9n), in which the nuclease domain RuvC is inactivated,[5] causes a single-strand nick. The combination of two single guide RNAs with the Cas9n causes one nick on each strand of the target sequence, thus inducing a DSB at the desired gene locus. (B) A pair of computationally predicted sgRNAs, targeting opposite strands of *KRT14* intron 7, 188 and 200 nt downstream of the missense mutation (c.1231G>A) within exon 6 (red star), with an sgRNA offset of +23 bp, mediates DSBs with 57-bp-long 5′ overhangs.

The CRISPR/Cas9 technology has enormous potential in the development of gene therapies for monogenic disorders. Epidermolysis bullosa simplex (EBS) is a rare genetic condition that is caused primarily by mutations in either the keratin 14 (*KRT14*) or keratin 5 (*KRT5*) gene. The intermediate filament proteins encoded by these genes are expressed in keratinocytes within the basal epidermal layer, and deleterious mutations in either impair cellular stability, resulting in cytolysis even upon minor external friction, thereby leading to blister formation. EBS is the most frequently occurring subtype of EB, with an incidence of approximately 1 case per 25,000 live births.[8–10] In the generalized-severe subtype of EBS (EBS-gen sev), the vast majority of mutations are either missense or small in-frame insertions or deletions (indels),[11] acting in an autosomal dominant manner. These mutations mainly affect the helix initiation motif or the helix termination motif of the keratin rod domain, which play crucial roles in the formation of the heterodimers resulting in intermediate filament instability and the characteristic presence of cytoplasmic aggregates containing mutant keratin.[10] Considering the dominant negative effect of mutant keratins on the intermediate filament cytoskeleton, therapies for the dominantly inherited EBS-gen sev subtype are limited and cannot be addressed by simple gene-replacement strategies. Rather, causal therapies must not only supply a wild-type gene, but also downregulate the disease-causing allele.

In the present study, we describe a CRISPR/Cas9n-mediated double-nicking strategy for the specific repair of a dominant mutation within exon 6 of the *KRT14* gene in a patient keratinocyte line. Double-nicking-mediated DNA cleavage was recently described to be a versatile

gene-editing strategy with an improved safety profile in comparison with the commonly used introduction of DSBs by wild-type spCas9 nuclease associated with considerable off-target activity.[5,12,13] While the usage of the nickase Cas9n is known to facilitate HDR at the target region,[14] the combined application of two nickases in a double-nicking configuration further improves its efficiency, which is, in single-nicking approaches, substantially reduced in comparison with the wild-type spCas9.[5] We targeted *KRT14* intron 7 by simultaneous single-nicking on both DNA strands (double-nicking) and offering a homologous wild-type donor template at the same time. Correction of the mutation via HDR was confirmed, resulting in a full rescue of the EBS phenotype in vitro, as shown by a normalization of the overall *KRT14* expression and the absence of K14 aggregates upon heat shock.[15]

RESULTS

Selection of a Specific Guide RNA Pair for DSB Induction

To establish a strategy for correction of a dominantly inherited hotspot missense mutation (c.1231G>A) within exon 6 of the *KRT14* gene[16,17] using CRISPR/Cas9 and HDR, we initially evaluated both the wild-type Cas9 nuclease from streptococcus pyogenes (spCas9) and its modified variant D10A (Cas9n) for DNA cleavage efficiency at the selected *KRT14* target site. Ran et al.[5] successfully performed double-nicking-mediated gene targeting with an efficient offset distance between the PAM-distal (5′) ends of both sgRNA sequences of up to 100 bp. To reduce the risk of nuclease-mediated mutagenesis of coding regions, we decided to screen for sgRNAs targeting an intronic region next to the mutation. Therefore, we screened intron 6 for suitable sgRNAs, which could further be used for our double-nicking approach. Unfortunately, we could not identify a suitable sgRNA pair for intron 6. However, we were able to predict a pair of suitable sgRNAs that bind with an offset of 23 bp to a region within *KRT14* intron 7 located 188–200 nt downstream of the causal mutation.[18] sgRNA1 and sgRNA2 was the closest sgRNA pair downstream of the mutation that fulfilled the current criteria for efficient double-nicking.[5] Co-delivery of sgRNA1 and sgRNA2 in combination with Cas9n into the target cells is predicted to induce DSBs with 57-bp-long 5′ overhangs (Figure 1B). We analyzed the functionality of our selected sgRNAs by delivering the respective spCas9/sgRNA expression plasmids into HEK293 cells and performing a T7 endonuclease I (T7EI) assay on the PCR-amplified *KRT14* target region.[19,20] T7EI recognizes and cleaves DNA at sites of base pair mismatches, such as those formed upon NHEJ repair of DSBs. As such, the T7EI assay serves as an indirect test for DSB and NHEJ induction. Depending on the nuclease cutting site within *KRT14* intron 7, the PCR-amplified target region was fragmented into two pieces of 312 and 183 bp (spCas9/sgRNA1) and 375 and 120 bp (spCas9/sgRNA2), respectively, confirming the ability of both sgRNAs to direct wild-type spCas9 to the target site for induction of DSBs. In contrast, when co-delivering sgRNA1 and sgRNA2 in combination with the modified Cas9n into HEK293 cells (double-nicking approach), we observed minimal levels of T7EI-mediated cleavage (Figure 2A, left panel), suggesting a general low efficiency of DSB induction via this approach. We confirmed these results by NGS of the PCR-amplified *KRT14* region, which revealed a general NHEJ induction efficiency of up to 16% for the spCas9/sgRNA1 and 30% for the spCas9/sgRNA2 at locations immediately adjacent to the PAM sequence (+2 to +4 nt) (Figure 2B, left panel), which was reduced to undetectable levels in the double-nicking approach.

Specificity Test Revealed No Off-Target Effects for the Double-Nicking Approach

The double-nicking strategy utilizing two separate sgRNAs in combination with Cas9n has recently been described to result in reduced off-target activity in comparison with sgRNA/wild-type spCas9 approaches.[5] To confirm this, we analyzed the DNA cleavage activity of these respective nucleases at several potential off-target regions, identified by BLAST analysis, for sgRNA1 and sgRNA2 (Table S1; Figure S1). Of note, sgRNA1 is highly homologous to a region within intron 10 of *TACC3*, differing by only 1 nt within the predicted PAM sequence, making this locus a potential target for this sgRNA. Indeed, DNA DSB induction by spCas9/sgRNA1 at this site was confirmed by T7EI assay showing digestion of the amplified *TACC3* region into two fragments of 407 and 213 bp upon T7EI treatment (Figure 2A, right panel). sgRNA2, which shares no homology to *TACC3*, was unable to direct spCas9 to induce DNA DSBs within this locus as demonstrated by the T7EI assay, and cells treated with the double-nicking constructs were also negative in this assay (Figure 2A, right panel). NGS analysis further verified the generation of deletions within intron 7 of *KRT14* and intron 10 of *TACC3* caused by spCas9/sgRNA1, which differed neither in position nor in deletion size (Figure 2C). However, indels were undetectable for Cas9n/sgRNA1 and sgRNA2 at the *TACC3* locus, underscoring the specificity and safety advantage of the double-nicking approach, which requires both sgRNAs to bind in close proximity to each other to generate a DSB. For all other predicted off-target genomic loci, we observed no or, if any, <3% (as for *RAP1GAP2* intron 2) indel formation by either spCas9/sgRNA (Table S1). All values (% indels of total reads) were at or near the baseline calculated from NGS data obtained from untreated HEK293 cells.

Thus, our results demonstrate that the double-nicking Cas9n approach is less efficient in inducing DSBs than the wild-type spCas9/sgRNA approaches. However, because of the reduced off-target activity of the double-nicking approach, which is an important prerequisite for any future clinical application, we decided to proceed with the Cas9n/sgRNA1 and sgRNA2 configuration for subsequent gene correction studies in EBS keratinocytes.

HDR-Mediated Gene Repair Using an MC System

To achieve HDR of the causal heterozygous mutation (c.1231G>A) within exon 6 of *KRT14* in a patient-derived EBS human keratinocyte line (EBS hKc), we first generated a minicircle (MC) vector that carries the homologous donor template extending from intron 3 to the 3′ UTR of *KRT14*. The MC vector lacks any bacterial backbone, resulting in an overall vector size reduction from ~8,000 (parental vector) to ~3,500 bp (MC) (Figure S2A). This results in increased transfection efficiency into cells when compared with standard

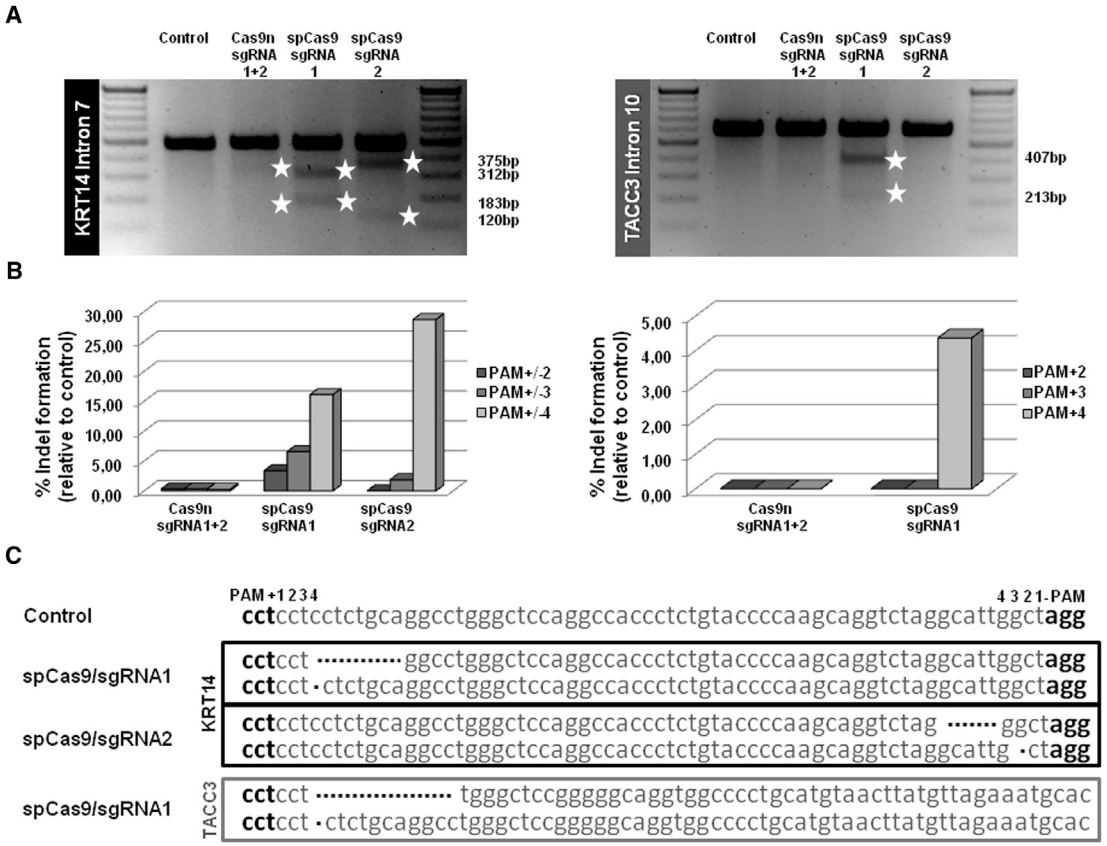

Figure 2. Specificity Test of Selected sgRNAs Using T7EI Assay and NGS Analysis

(A) Upon delivery of the respective spCas9/sgRNA (sgRNA1 and sgRNA2) expression plasmids into HEK293 cells, the target region was PCR-amplified using a primer pair binding specifically to *KRT14* exon 6 and intron 7. The resulting PCR products were cleaved by T7EI treatment into two fragments, 312 and 183 bp for sgRNA1 and 375 and 120 bp for sgRNA2, thus confirming the on-target functionality of both sgRNAs. In the double-nicking approach, both sgRNAs were transfected in combination with Cas9n, resulting in the desired T7EI digestion pattern detectable via agarose gel analysis. The resulting digest pattern is a mixed pattern derived from both sgRNAs (fragments between 375 and 312 bp, and fragments between 183 and 120 bp). The predicted off-target region for sgRNA1 was PCR-amplified using a primer pair binding specifically within *TACC3* intron 10. The resulting PCR products were cleaved by T7EI treatment into two fragments of 407 and 213 bp confirming the predicted off-target activity of sgRNA1 when combined with the wild-type spCas9. (B) Relative cutting efficiencies of different Cas9 enzymes were determined by next generation sequencing. Using a custom-designed panel for on/off-target analysis of the *KRT14* target region and predicted off-target regions of the selected sgRNAs, the relative amount of indel formation at intron 7 of *KRT14* (left panel) and intron 10 of *TACC3* (right panel) was analyzed. The graphs show the relative amount of indels compared with untreated control. (C) Sequences of NGS analysis showing mainly small deletions of 1–20 bp for each spCas9/sgRNA at the *KRT14* and *TACC3* locus.

plasmids (Figure S2B), which is expected to be associated with an enhanced HDR efficiency because of an increased availability of HDR donor templates. The MC included engineered restriction sites for EcoRI and NheI within intron 7, which were included to facilitate the quantification of recombination events. Additionally, a GFP-IRES-blasticidin selection cassette under the control of the EF1 promoter was incorporated downstream of the *KRT14* 3′ UTR for initial selection of transfected cells (Figure 3). The MC was co-transfected into EBS hKc cells together with spCas9/sgRNA1, spCas9/sgRNA2, or Cas9n/sgRNA1 and sgRNA2. To more accurately determine HDR efficiency achieved with our double-nicking approach compared with the spCas9 approaches and to exclude differences due to different transfection efficiencies, we pre-selected our treated cell population with blasticidin, to maintain a homogeneous cell population carrying the transfected vectors. We achieved a transfection efficiency of ~30% into EBS hKc cells as estimated by the analysis of GFP expression via flow cytometry. Following blasticidin selection, ~90% of EBS hKc were GFP-positive (Figure S2C). For analysis of HDR-mediated integration of donor template sequences, PCR amplification of genomic DNA from treated patient cells was performed using a forward primer that specifically binds the integrated restriction sites EcoRI and NheI and a reverse primer binding downstream of the *KRT14* 3′ UTR, in a region not present in the MC vector. Thus, amplification of the MC donor template is excluded by this strategy. We observed a PCR product of the expected size of 893 bp under all conditions tested, revealing the accurate, HDR-mediated integration of these restriction sites within intron 7 of *KRT14* (Figure 4A). In order to more accurately assess the HDR efficiency achieved under the different gene-editing conditions tested, we performed a separate PCR using primers specifically amplifying the *KRT14* region

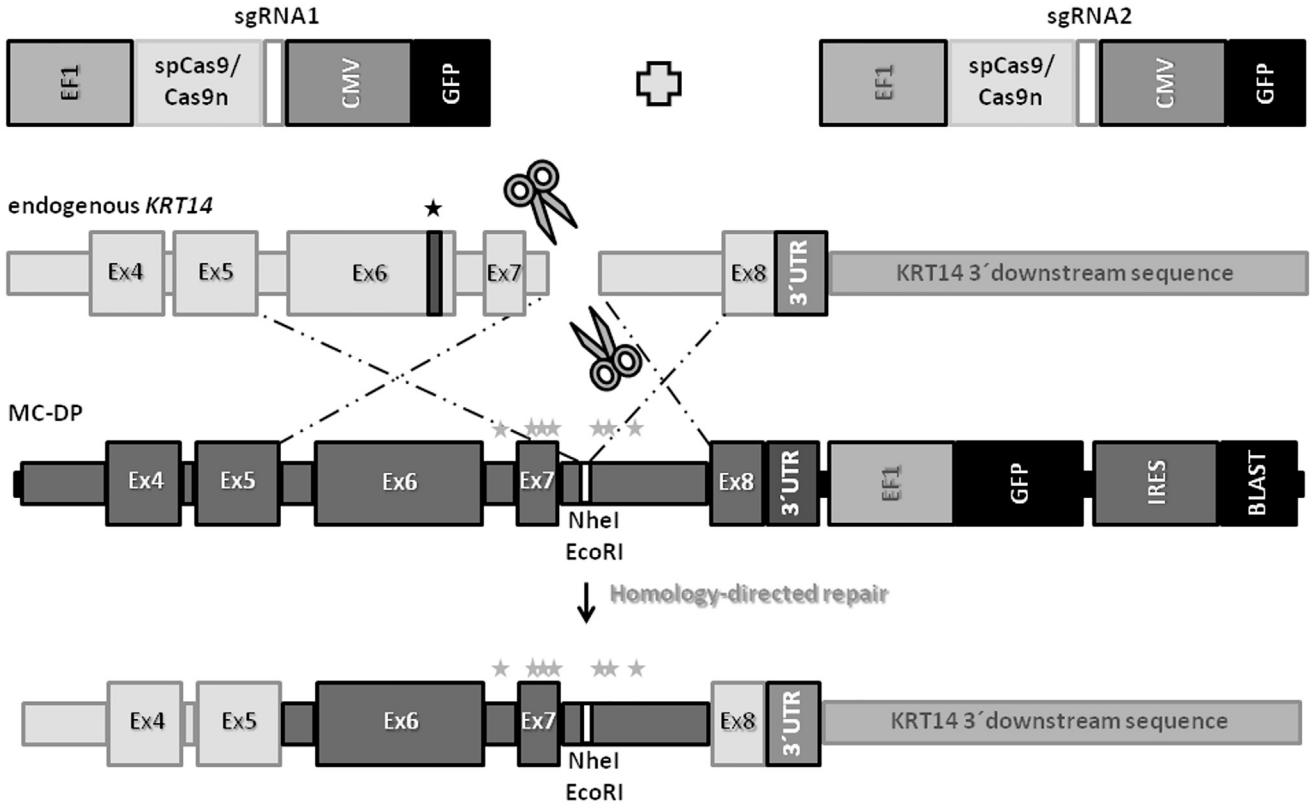

Figure 3. HDR of *KRT14* Using an MC-Based System

Co-transfection into EBS hKc of the respective Cas9/sgRNA combination (spCas9-sgRNA1, spCas9-sgRNA2, or both Cas9n-sgRNA1 and Cas9n-sgRNA2) and the MC donor plasmid, carrying the homology donor template spanning from intron 3 to the 3′ UTR of *KRT14* and a GFP-IRES-blasticidin under the control of an EF1 promoter, led to DSB induction within intron 7 of *KRT14* and subsequently to the HDR-mediated introduction of the silent mutations (gray stars) and two restriction sites provided by the MC donor vector, and the repair of the dominant disease-causing mutation (black star).

spanning exon 6 to 60 nt downstream of the 3′ UTR, which again excludes amplification of the MC vector and results in a product of 1,189 bp. Digestion of this PCR product (1,189 bp) with EcoRI generated the expected cleavage products of 874 and 315 bp that were readily detectable only in the double-nicking approach, indicating a higher HDR efficiency compared with the spCas9/sgRNA approaches (Figure 4B).

HDR Efficiency upon Double-Nicking-Induced DNA Cleavage

To evaluate the relative HDR efficiency in blasticidin-selected EBS hKc treated with the double-nicking constructs, the PCR-amplified *KRT14* target region was subcloned into an appropriate subcloning DNA vector for transformation into competent bacterial cells and analysis of resulting colonies. To increase the subcloning efficiency, we first performed a nested PCR on the initial integration-specific product (1,189 bp) spanning exon 6 to 60 nt downstream of the 3′ UTR, which excludes amplification of the MC vector, reducing the size of PCR product to be subcloned to 507 bp (Figure 5A). Colony PCR of single colonies and EcoRI restriction digestion of the amplified DNA resulted in the correct digestion pattern in 11 of 32 colonies, demonstrating an HDR efficiency of approximately 34% (Figure 5A, right panel).

For a more detailed analysis of the editing processes induced by the double-nicking approach, we picked a total of 96 bacterial colonies and performed sequence analysis on the resulting colony PCR products. This revealed an HDR efficiency of up to 32% (Figure 6B), in keeping with results from the restriction digestion assay above. Silent mutations introduced into both homologous *KRT14* arms allowed us to assess sites preferentially used for recombination, which seem to be located within the 5′ region of the *KRT14* donor template (Figure 6C). Sequencing analysis further revealed NHEJ indel formation of 47%, which can be subdivided into 38% deletions and 9% insertions. Finally, we observed a ratio of wild-type /mutation allele of 63/33. Assuming a wild-type/mutation allele ratio of 50/50 in untreated patient keratinocytes, we calculated a mutation correction efficiency of approximately 16% with the double-nicking approach (Figure 6A).

Off-Target Site Analysis in EBS Keratinocytes

To reconfirm the specificity of our double-nicking approach, we performed NGS on genomic DNA isolated from treated and blasticidin-selected EBS keratinocyte bulk populations. NGS of the PCR-amplified on-target *KRT14* region revealed a general NHEJ induction efficiency of up to 10% for our double-nicking approach, 2% for the

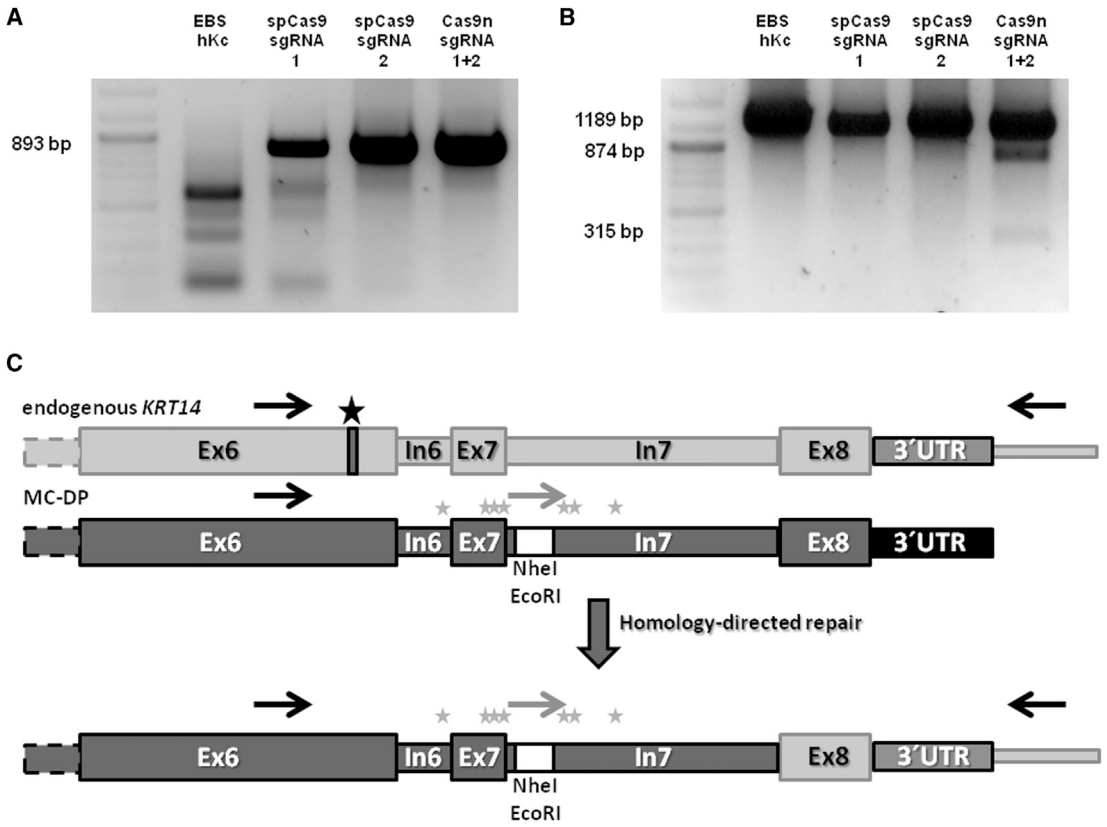

Figure 4. Integration and HDR Analysis of CRISPR/Cas9-Edited EBS hKc

After co-transfection of the respective Cas9/sgRNA combinations (spCas9-sgRNA1, spCas9-sgRNA2, or both Cas9n-sgRNA1 and Cas9n-sgRNA2) and the MC donor plasmid into EBS hKc, we performed two rounds of blasticidin selection. The resulting blasticidin-resistant cells were then analyzed for site-specific integration of the donor template at the genomic level. (A) Integration-specific PCR using a forward primer binding the restriction sites EcoRI and NheI (white box) provided by the MC and a reverse primer binding downstream to the 3′ UTR of the *KRT14* gene resulted in a PCR product of 893 bp. (B) EcoRI digestion to estimate the relative recombination efficiency in the treated cell pool. We performed a PCR using a forward primer binding to exon 6 and a reverse primer binding a sequence downstream of *KRT14* 3′ UTR. The PCR resulted in a specific product of 1,189 bp. EcoRI digestion generated the expected fragments of 874 and 315 bp, only visible in the Cas9n 1- and 2-treated EBS hKc. (C) Schematic depiction of the primer binding sites used for amplification of the integration-specific PCR fragments. Gray arrows indicate a forward primer binding to the restriction sites EcoRI and NheI integrated via HDR. Black arrows indicate forward and reverse primers binding to endogenous *KRT14*. Black star: missense mutation (c.1231G>A) in exon 6; gray stars: silent mutations.

spCas9/sgRNA1 and 32% for spCas9/sgRNA2, respectively (Figure 7A). The reduced number of NHEJ events detectable in the respective Cas9/gRNA-treated cell populations is due to the presence of the MC vector at the time point of sequence analysis, influencing the evaluation of the results (Figure 7). The NHEJ rates are therefore underestimated compared with NHEJ rates we obtained by the subcloning strategy (Figure 6) wherein amplification of the MC was excluded by the PCR strategy. To confirm the reduced off-target activity of the Cas9n in comparison with the wild-type spCas9 nuclease, we analyzed the DNA cleavage activity of the respective nucleases at the potential off-target regions for sgRNA1 and sgRNA2 (Figure 7A) as already described above. NGS analysis revealed deletions within intron 7 of *KRT14* and intron 10 of *TACC3* in cells treated with spCas9/sgRNA1, as expected. Additionally, NGS analysis of two predicted off-targets for sgRNA2 indicated possible DNA cleavage activity. However, in cells treated with the double-nicking constructs, only indels within intron 7 of *KRT14*, but not within any predicted off-target region, including intron 10 of *TACC3*, were detectable, again emphasizing the improved safety profile of our double-nicking approach (Figure 7B). Treatment of cells with the double-nicking constructs resulted in deletions located between the binding sites of both sgRNAs, but further away from the PAM sequences, and they were larger in size compared with deletions resulting from spCas9/sgRNAs (Figure 7C).

Corrected EBS Single-Cell Clones Exhibit Reversion of Disease Phenotype

Our results thus far demonstrate an HDR efficiency of up to 32% and a mutation correction efficiency of approximately 16% in pre-selected EBS keratinocytes by our double-nicking approach. In order to demonstrate that correction of the causal mutation results in the reversion of the EBS disease phenotype, we first isolated single cells

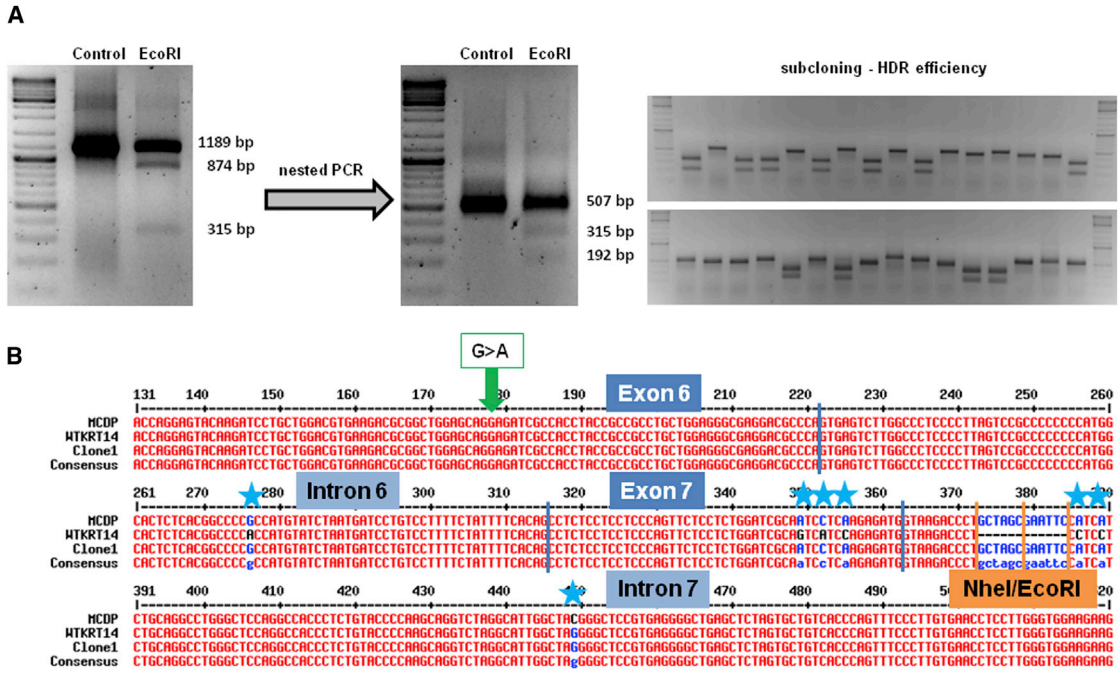

Figure 5. Analysis of HDR Efficiency

(A) PCR analysis of genomic DNA from CRISPR/Cas9-treated EBS hKc using a forward primer binding to exon 6 and a reverse primer binding a sequence downstream of *KRT14*. To minimize the size of the PCR product and to facilitate subcloning, we performed a nested PCR using a forward primer binding to exon 6 and a reverse primer binding to intron 7, resulting in a specific product of 507 bp. An EcoRI restriction digest confirmed the presence of recombined *KRT14* alleles in treated EBS cells. Upon bacterial transformation, single colonies were picked for colony PCR and amplified product digested with EcoRI to identify recombined alleles. (B) Sequence analysis of one representative single clone, containing a modified wild-type allele (green arrow: wild-type sequence at mutation site [position 178] within exon 6), is shown. The allele additionally contains the introduced restriction sites NheI/EcoRI and the silent mutations (blue stars). Sequence alignment was performed with the software "Multiple sequence alignment with hierarchical clustering."[21]

from the blasticidin-selected EBS bulk population. From 384 single cells initially isolated, we were able to maintain and expand a total of 17 clonal populations. 12 clones were screened via western blot analysis for keratin 14 (K14) expression, resulting in the identification of 5 clones showing restoration of normal K14 protein levels, 7 of which exhibited increased K14 levels characteristic of the parental EBS hKc cell line (data not shown). We chose two separate clones, clones 16 and 17, with opposite K14 profiles, for further analysis. PCR amplification of the *KRT14* target region from isolated genomic DNA and synthesized cDNA of the selected cell clones revealed correction of the mutation at genomic level and RNA level for single-cell clone 17, whereas there was no correction for single-cell clone 16 (Figures S3A and S3B). Both cell clones showed signs of CRISPR/Cas9 HDR-mediated gene editing. This was evident in the introduction of silent mutations engineered into the MC donor template. We also amplified the off-target region within intron 10 of *TACC3* and could again demonstrate the absence of indel formation within this predicted off-target site (Figure S3C).

EBS-gen sev keratinocytes accumulate K14 because of a positive autocrine feedback loop involving interleukin-1β (IL-1β) and the stress-related JNK pathway.[15,22] The incorporation of mutant K14 proteins into the intermediate filament network renders the network unstable and sensitive to minor stress, such as heat shock, resulting in its collapse into aggregates, which accumulate in the cytoplasm. Thus, correction of the causal mutation should restore intermediate filament stability and normalize K14 expression within the cell. In line with this, heat shock assays demonstrate the collapse of the intermediate filament network into aggregates in parental EBS hKc cells and in clone 16, which is completely absent in clone 17 (Figures 8A and 8B). Furthermore, whereas parental EBS hKc cells and the uncorrected clone 16 showed increased *KRT14* expression compared with wild-type hKcs, the corrected clone 17 showed a normalized *KRT14* expression pattern (Figures 8C and 8D). Thus, correction of the disease-causing mutation, as achieved here by HDR and CRISPR/Cas9 technology, results in the functional reversion of the EBS-gen sev-associated phenotype.

DISCUSSION

The generalized severe simplex subtype of EBS has an inflammatory phenotype caused by a single heterozygous mutation within either of the basal keratins that results in functionally impaired protein that interferes with the correct assembly of the intermediate filament network in basal keratinocytes.[15,22] As highlighted by the few clinical trials and case reports that have been published so far,[23–28] there are no established targeted/molecular treatment options for EBS, and

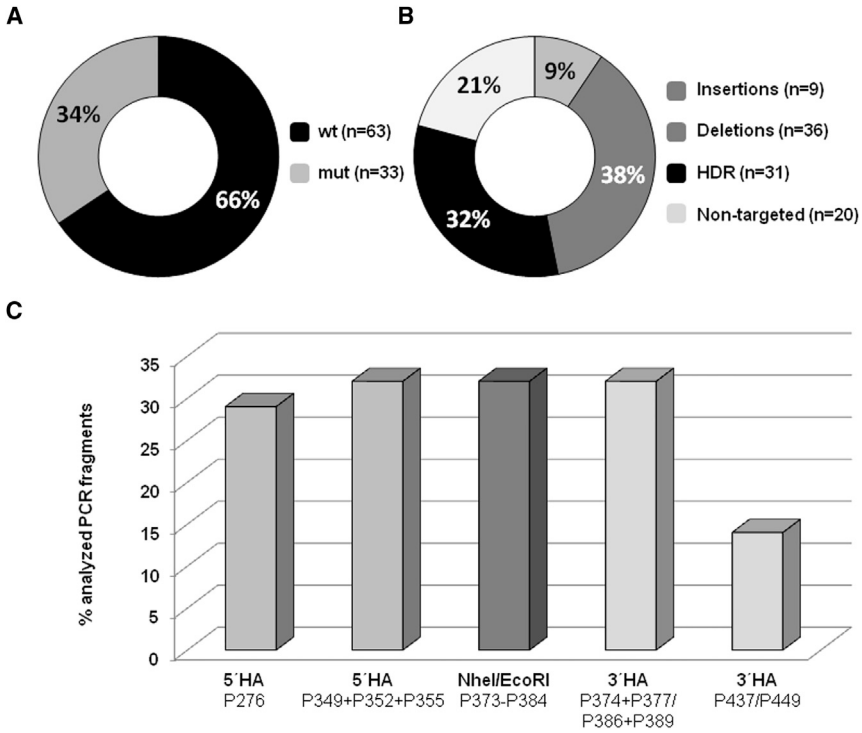

Figure 6. HDR Efficiency of the MC Double-Nicking Approach

96 subcloned nested PCR fragments were sequenced and analyzed. (A) Ratio between wild-type and mutated alleles. (B) Ratio between NHEJ (insertions and deletions) and HDR. n = absolute numbers of analyzed sequences. (C) HDR analysis. The position of sequence modifications (P) was defined according to the *KRT14* target sequence exon 6-intron 6-exon 7-intron 7 (exon 6: P1-P221; intron 6: P222-P315; exon 7: P316-P362; intron 7: P363-P923). wRS, with restriction sites (exon 6: P1-P221; intron 6: P222-P315; exon 7: P316-P362; intron 7: P363-P935).

current standard care for EBS-gen sev patients still focuses on wound care and symptomatic treatments. In general, therapeutic strategies for genetic diseases target either the genetic cause underlying a specific disorder or disease-specific pathophysiological pathways. For EBS, both causal and symptomatic treatment strategies have been investigated during the last decade. In order to identify potential targets for novel treatments, Wally et al.[15,29] investigated the EBS-gen sev pathomechanism, identifying the pro-inflammatory interleukin-1β (IL-1β)-mediated stress pathway to be constitutively activated. Disrupting IL-1β signaling with antibodies or the small molecule diacerein resulted in a reversion of the IL-1β-related gene expression signature toward the wild-type signature. Translation of this approach into a clinical setting resulted in a significant amelioration of the disease phenotype, i.e., a reduction of blister numbers, in EBS-gen sev patients.[15,29] While diacerein represents a specifically targeted, symptomatic, and potentially short-term accessible treatment option that has already taken steps forward into clinics, causal treatment approaches, such as spliceosome-mediated pre-mRNA *trans*-splicing (SMaRT), are still under development.[15] Causal treatment of monogenic diseases requires sustained replacement or correction of the affected gene or mRNA. In addition, considering the dominant negative effect of mutant keratins on the intermediate filament network, therapies for EBS-gen sev are limited, and conventional gene replacement strategies are not applicable. Even though progress has been made in the field of ex vivo gene therapy for other subtypes of EB (junctional and recessive dystrophic EB), for the dominantly inherited EBS-gen sev, this therapeutic approach is currently not available[30–32] because dominant negative interference cannot be overcome simply by providing a wild-type cDNA. Rather a significant reduction of mutated K14 determines the success of the treatment as it is the incorporation of this faulty molecule into the intermediate filament network that, upon stress, subsequently triggers filament aggregation.[22,33–35] Accordingly, success has also been achieved using short inhibitory RNAs (siRNAs) and therapeutic *trans*-splicing, both of which result in reduction in levels of the faulty transcript.[22,35] Permanent deletion or repair of the causal mutation at genomic level, using current state-of-the-art gene-editing tools such as TALEN or CRISPR/Cas9, would circumvent the need for repeated administration of transiently acting drugs. In this respect, Petek et al.[36] have already demonstrated that targeted alteration of a disease-causing *KRT14* allele using a gene-targeting vector with promoter trap design results in restoration of the intermediate filament cytoskeleton of EBS keratinocytes in a xenograft mouse model.

The potential to repair any mutation that causes a severe disease phenotype renders the CRISPR/Cas9 system an attractive and broadly applicable gene-editing tool. CRISPR/Cas9 constructs can be easily generated and adapted for almost any genomic region of interest. The main difficulty concern regarding a future clinical application is to predict off-target activity of the nuclease. Until now, low HDR efficiencies accompanied by high risks of off-target effects have impeded its way into the clinic as a curative treatment for monogenetic disorders.[12] Indeed, Fu et al.[13] showed frequent off-target mutagenesis induced by the commonly used spCas9 in human cells, exhibiting the need for both extensive sgRNA pre-selection and very sensitive off-target analysis tools. Therefore, recent studies have focused on the improvement of HDR efficiency and the safety profile of the commonly used spCas9 nucleases. Ran et al.[5] described a method to increase HDR rates and to reduce the frequency of off-target events by using the Cas9 mutant D10A (Cas9n), which preferably induces single-strand breaks (nicks) within the DNA, in a double-nicking configuration. Targeting opposite DNA strands separately to induce what is tantamount to DSBs within the desired region reduces the chance of unwanted indel formation elsewhere in the genome, a common side event observed with the wild-type spCas9.[5,12]

A

sgRNA 1	3´ggaggagacgtccggacccg 5´								
				Cas9n/ sgRNA1+2			spCas9/ sgRNA1		
localization	target sequence								
on-target sgRNA1	on-target sgRNA1	PAM+2	PAM+3	PAM+4	PAM+22	PAM+23	PAM+2	PAM+3	PAM+4
KRT14 Intron 7 (sense)	5´cctcctcctctgcaggcctgggc 3´	0,01	0,00	0,00	10,51	10,15	1,01	0,96	1,91
off-targets sgRNA1	off-targets sgRNA1	PAM+/- 2	PAM+/- 3	PAM+/- 4	PAM+22	PAM+23	PAM+/- 2	PAM+/- 3	PAM+/- 4
TACC3 Intron 10 (sense)	5´ccccctcctctgcaggcctgggc 3´	0,08	0,10	0,00	0,03	0,00	3,12	3,21	2,09
APP Intron 7 (antisense)	3´ctacataattcgtctcctcctcc 5´	0,00	0,00	0,07	0,00	0,06	0,00	0,00	0,43
ITGB2 Intron 4 (antisense)	3´ttaaggtccgcgtctcctcctcc 5´	0,00	0,00	0,00	0,00	0,00	0,00	0,00	0,03
RAP1GAP2 Intron 2 (sense)	5´cctcctcctctgctggccttccac 3´	0,03	0,12	0,00	0,00	0,00	0,07	0,13	0,00
ABCG1 Intron 14 (sense)	5´gagcctcctctgcaggaggccag 3´	0,00	0,00	0,00	0,00	0,10	0,00	0,00	0,12
PDXK Intron 4 (sense)	5´cttcctcctctgcacgcctccgt 3´	0,00	0,00	0,00	0,00	0,02	0,00	0,00	0,00
IGSF5 Intron 7 (sense)	5´actcctcctctgcaggatgaaca 3´	0,00	0,03	0,02	0,00	0,00	0,10	0,19	0,03
HLCS Intron 1 (antisense)	3´gatgctcctctgcaggccgcagg 5´	0,00	0,00	0,00	0,12	0,13	0,00	0,00	0,00
sgRNA 2	5´agcaggtctaggcattggct 3´								
				Cas9n/ sgRNA1+2			spCas9/ sgRNA2		
localization	target sequence								
on-target sgRNA2	on-target sgRNA2	PAM-2	PAM-3	PAM-4	PAM-41	PAM-42	PAM-2	PAM-3	PAM-4
KRT14 Intron 7 (antisense)	3´tcgtccagatccgtaaccgatcc 5´	0,20	0,23	0,00	10,51	10,15	0,18	1,09	32,44
off-targets sgRNA2	off-targets sgRNA2	PAM+/- 2	PAM+/- 3	PAM+/- 4	PAM-41	PAM-42	PAM+/- 2	PAM+/- 3	PAM+/- 4
SLC22A18 Intron 6 (antisense)	3´ccgttaccttccgtaaccgatcc 5´	0,01	0,11	0,00	0,06	0,00	0,00	0,00	0,00
TMPRSS11D Intron 1 (sense)	5´cctagccaatgccttcctaggaa 3´	0,00	0,30	0,00	0,04	0,00	0,00	0,20	0,00
ANK2 Intron 1 (antisense)	3´cttaataaacccgtaaccgatcc 5´	0,12	0,03	0,05	0,00	0,32	0,81	0,69	0,00
AAMDC Intron 3 (antisense)	3´accccaatatccgtaaccgattt 5´	0,05	0,00	0,00	0,29	0,00	0,00	0,00	0,00
SLC1A3 Intron 3 (antisense)	3´acttagatatccgtaaccgatta 5´	0,00	0,00	0,00	0,00	0,00	0,21	0,17	1,05

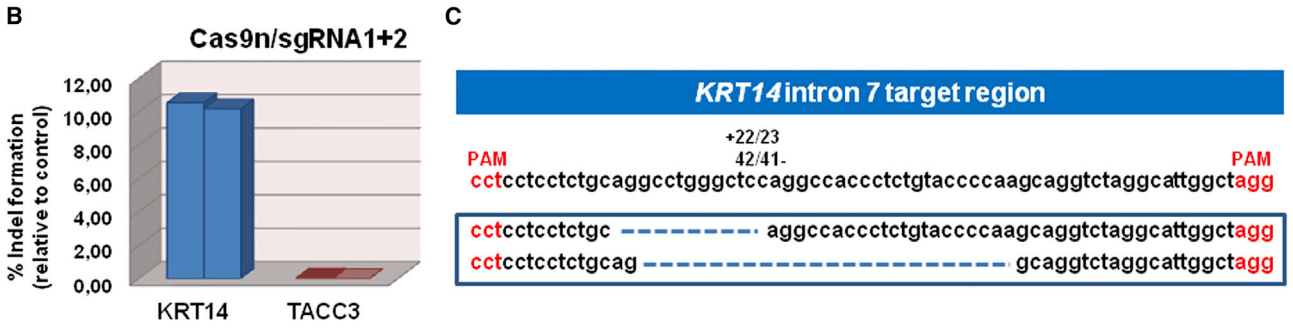

Figure 7. Specificity Test of Selected sgRNAs in an MC-Treated EBS hKc Cell Line Using NGS

(A) DNA cleavage activities of sgRNAs at on-target and off-target regions are represented as % indels relative to untreated control. The cutoff for cleavage activity was set to 0.5%. Colored boxes indicate cleavage activity of the respective Cas9/sgRNAs at on-target and off-target regions. On-target and off-target region sequences are listed, with red letters indicating the PAM position, blue letters indicating mismatches between the sgRNA on-target binding sites and the potential off-target regions, and black letters indicating matches between on-target and off-target regions. (B) Graphs show the relative amount of indels (PAM +22/23) within *KRT14* intron 7 and *TACC3* intron 10, caused by double-nicking compared with untreated control. (C) Sequences of NGS analysis showing frequent deletions for the Cas9n/sgRNA1 and Cas9n/sgRNA2 configuration.

In this study, we demonstrate the feasibility of this approach in the HDR-mediated correction of a dominant hotspot mutation within the *KRT14* gene, which is associated with the EBS-gen sev phenotype. The site chosen for DSB induction was determined by the presence of PAM sequences on both DNA strands spaced 23 bp apart and is located ~200 bp downstream of the mutation within intron 7 of *KRT14*. Even though the relatively large distance to the mutation is expected to reduce the general repair efficiency, we chose the double-nicking strategy because of safety concerns. Besides the auspicious safety profile of the Cas9n nickase, targeting an intron reduces the risk for nuclease-mediated mutagenesis of coding sequences.

Using this approach, we achieved HDR efficiencies of up to 32% in pre-selected EBS patient keratinocytes accompanied by an overall mutation correction rate of approximately 16%. Furthermore, corrected single-cell clones showed a restored K14 expression pattern. A heat shock assay confirmed successful correction at the functional level, as demonstrated by the absence of the characteristic EBS-gen sev K14 aggregates, indicating restoration of the stability of the intermediate filament network. The double-nicking approach is not only an example for what can be accomplished with CRISPR/Cas9, but also shows proof-of-principle for the repair of dominant mutations.

A major aspect of our study is the development of a safe repair strategy. Additional to commonly used T7EI assays and surveyor assays, we performed an extended off-target analysis via NGS. The off-target analysis via T7EI assay and NGS indicates adverse effects caused by the wild-type spCas9/sgRNA1 and wild-type spCas9/sgRNA2, respectively, at predicted target regions highly homologous to the respective sgRNA binding sequence. However, this was not detectable in the double-nicking approach, rendering this the safest and most

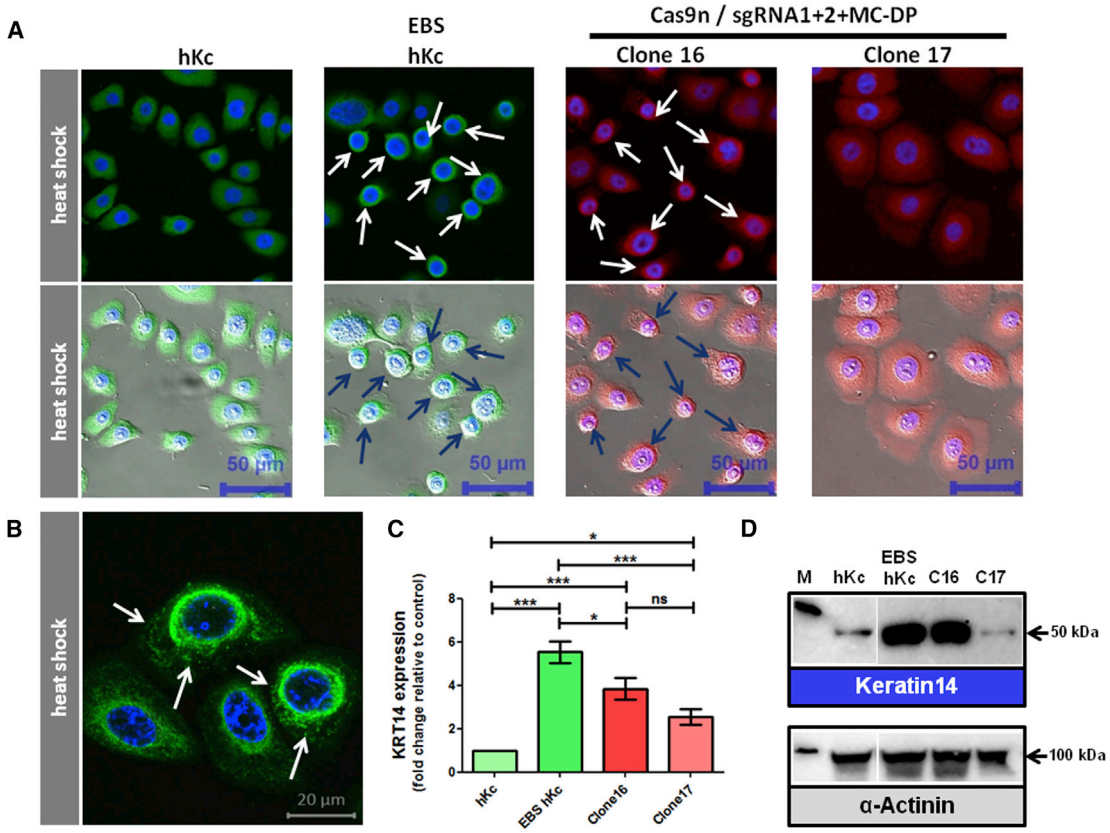

Figure 8. CRISPR/Cas9-Mediated Reversion of Disease Phenotype in EBS Single-Cell Clones

(A) Immunofluorescence staining using antibodies directed against K14 upon 30 min of heat stress (43°C) followed by 15 min recovery time at 37°C in CRISPR/Cas9-treated EBS keratinocytes. Human keratinocytes and EBS keratinocytes served as controls. K14 staining showed a full reversion of the disease-associated K14 aggregation in Cas9n-sgRNA1 and Cas9n-sgRNA2/MC-DP-treated single-cell clone 17. EBS hKc and the uncorrected Cas9n-sgRNA1 and Cas9n-sgRNA2/MC-DP-treated single-cell clone 16 showed the characteristic K14 aggregates around the nucleus and the periphery of the cytoplasm (arrows), which are not visible in human wild-type keratinocytes (hKc) and Cas9n/sgRNA1 and 2/MC-DP repaired EBS patient keratinocytes (scale bar, 50 µm). (B) Typical cytokeratin 14 aggregate formation (white arrows) in EBS cells upon heat stress (scale bar, 20 µm). (C) mRNA expression levels of *KRT14* in wild-type hKc, CRISPR/Cas9-treated, and nontreated EBS patient keratinocytes via semi-quantitative real-time PCR. Expression levels were normalized to GAPDH. Relative expression levels were shown as fold change. The gene expression levels in human wild-type keratinocytes (hKc) were set to 1. Nine different runs with duplicates were analyzed using three different RNA samples of each cell line. Statistics were performed using the one-way ANOVA-Tukey's multiple comparison test. (D) Western blot analysis on whole cell extracts revealed a normalization of K14 for clone 17 at protein level compared with untreated EBS hKc and clone 16, which showed no correction of the causal mutation. α-Actinin was included as loading control.

feasible of all strategies tested here for the specific gene editing of *KRT14*. Although the frequency of DSB induction was significantly lower than in the single cutting approaches using the spCas9 nuclease, HDR efficiency was increased, making this strategy auspicious for future investigations in primary patient keratinocytes into which plasmid delivery is a key issue. In this respect, further improvements of the double-nicking strategy described here can include a direct Cas9 RNA or protein delivery into the cells, reducing the time of nickase activity, and thereby further reducing the frequency of off-target events. However, prior to translating our approach into the clinics, the risk of adverse off-target activity has to be extensively addressed by NGS. Specifically, whole-genome sequencing can further increase the sensitivity of the off-target analysis as it has already been shown for CRISPR/Cas9- and TALEN-edited human induced pluripotent stem cells (IPSCs) by Smith et al.[37]

The possibility to apply this gene-editing tool as an ex vivo gene therapy for patients suffering from blistering skin diseases further improves its safety profile. The ex vivo gene therapy will rely on the correction of autologous stem cells isolated from patients, which are further expanded to epidermal sheets and transplanted back. Modified stem cells can be clonally selected upon treatment, thereby increasing the ability to assess the safety profile of the approach significantly.[38,39] Epidermal sheets can be expanded from gene-corrected cells and subsequently transplanted back onto the patient, successfully demonstrating the high therapeutic potential of ex vivo gene therapy in the skin.[30–32] Considering that the mutational hotspots for EBS-gen sev are located in exons 1 and 6 of the *KRT14* gene, it is possible to treat the cells of multiple individuals from different families with a small set of designed sgRNA pairs, simplifying the therapeutic approach in this patient group. A CRISPR/Cas9n

ex vivo gene therapy treatment would offer a safe, effective, and, compared with other treatment options, permanent repair of the EBS skin. In many cases, EBS-gen sev is severe in childhood, but improves with age. However, specific sites of the body, such as the soles of the feet, are particularly prone to blistering, causing substantial pain throughout life. Ex vivo gene therapy could provide an additional and permanent treatment option for this patient population.

In summary, we here present an efficient and specific gene-editing approach for *KRT14* repair, which can be further translated into a clinical setting offering a causal treatment for patients suffering from severe skin blistering diseases.

MATERIALS AND METHODS

Selection and Cloning of sgRNA Specific for Intron 7 of KRT14

Putative sgRNA target sites within intron 7 of the *KRT14* gene were predicted using the online prediction platform CHOPCHOP.[18] The sgRNAs were designed (sgRNA1: 5′- ATCCGCCCAGGCC TGCAGAGGAGG-3′/5′-AAACCCTCCTCTGCAGGCCTGGGC-3′ and sgRNA2: 5′-ATCCAGCAGGTCTAGGCATTGGCT-3′/5′-AA ACAGCCAATGCCTAGACCTGCT-3′) and cloned as double-stranded oligonucleotides into either the CMV-T7-hspCas9-T2A-GFP-H1-gRNA CAS740G-1 linearized SmartNuclease vector or the CMV-T7-hspCas9-nickase-T2A-GFP-H1-gRNA CAS790G-1 linearized SmartNickase vector (System Bioscience, Palo Alto, CA, USA) according to the manufacturer's protocol.

Generation of the MC Donor Plasmid

The *KRT14* homology donor template was PCR-amplified in two fragments for ease of cloning into the MN511A1 vector (System Bioscience, Palo Alto, CA, USA). The first fragment was amplified using an intron-3-specific forward primer (5′-GATCTCTAGAGTGA GAACTATATGGAAAAGTCAGCTTAAAAGAAATGC-3′) and an intron-7-specific reverse primer (5′- GATCGCTAGCAGGGTC TTACCATCTCTTGAGGATTGCGATCCAGAGG-3′) and cloned into the MN511A1 vector via the XbaI and NheI sites incorporated within the primers. The resulting 1,173 bp fragment incorporates silent mutations within exon 7. The second fragment (805 bp) was amplified using an intron-7-specific forward primer, which incorporates three silent mutations (5′- GATCGAATTCCATCATCTGCA GGCCTGGGCTCCAGGCCACCCTCTGTACCCCAAGCAGGTC TAGGCATTGGCTACGGGCTCCGTG-3′) and a *KRT14* 3′ UTR-specific reverse primer (5′-GATCGGATCCTTATGCAACTCAG ATAATGAAGCTGTATTGATTG-3′), and subsequently cloned into EcoRI and BamHI restriction sites. Correct cloning was confirmed by sequence analysis. The resulting homology donor template encompasses the entire *KRT14* region from intron 3 to the 3′ UTR and incorporates NheI and EcoRI sites within intron 7, which facilitates detection of the recombined allele. The IRES-blasticidin cassette was cloned downstream of the *KRT14* 3′ UTR according to Peking et al.[40] For production of MC DNA, the MC-Easy-Minicircle DNA production kit (System Bioscience, Palo Alto, CA, USA) was used according to the manufacturer's protocol.

Transient Transfection of Donor Plasmids

The embryonic kidney cell line HEK293 (Stratagene, La Jolla, CA, USA) was cultivated in DMEM supplemented with 10% fetal bovine serum (FBS) and 100 U/mL penicillin/100 µg/mL streptomycin (Biochrom, Berlin, Germany). Human EBS keratinocytes (EBDM-2) carrying a heterozygous mutation (c.1231G>A) in exon 6 of *KRT14* and normal hKcs were cultivated in keratinocyte serum-free medium (SFM) GIBCO (Invitrogen, Paisley, UK) supplemented with bovine pituitary extract (BPE), epidermal growth factor (EGF) according to manufacturer's protocol, and 100 U/mL penicillin/100 µg/mL streptomycin. All cell lines were maintained at 37°C and 5% CO_2 in a humidified incubator.

Transient transfections of HEK293AD cells were performed using jetPEI reagent (Polyplus-transfection SA, Strasbourg, France), whereas transient transfections of EBS patient keratinocytes were performed using Xfect transfection reagent (Takara Bio Europe, Saint-Germain-en-Laye, France) according to the manufacturer's protocol. HEK293AD cells were cultivated in 60 mm plates and transfected with the respective Cas9/sgRNA-expressing plasmids (5 µg). Human EBS keratinocytes were transfected with the respective Cas9/sgRNA-expressing plasmids and the MC donor template in a ratio of 2:1 (4 µg DP and 2 µg sgRNA) or in the case of double-nicking in a ratio of 2:1:1 (4 µg DP and 2 µg of each sgRNA). Antibiotic selection of transfected EBS keratinocytes was performed when cells reached 60% confluency, by supplementing the medium with 10 µg/mL blasticidin (Invivogen, San Diego, CA, USA). Untransfected EBS keratinocytes cells were used as a negative control. For transfection efficiency tests of our different donor plasmids into EBS keratinocytes, cells were cultured in six-well plates and transiently transfected with 4.5 µg of plasmid using Xfect transfection reagent.

Flow Cytometric Analysis and Fluorescence-Activated Cell Sorting

Transfection efficiency was evaluated 48 hr post-transfection via flow cytometric analysis using a Beckman Coulter FC500 FACS (fluorescence-activated cell sorting) analyzer (Beckman Coulter, Brea, CA, USA). GFP (expressed from Cas9/sgRNA vector)-expressing cells were analyzed using the Kaluza Flow Cytometry Analysis Software (Beckman Coulter).

Isolation of Single-Cell Clones

To obtain a homogeneous cell population upon genome editing, we isolated single-cell clones using single-cell dilution. Cells were counted using a TC20 cell counter (Bio-Rad, Hercules, CA, USA) and manually seeded to obtain 0.5 cell per well of a 96-well plate in co-culture with 3T3-J2 mouse fibroblasts feeder cells (5×10^2 cells/cm^2) growth arrested with 4 µg/mL mitomycin C (Roche, Basel, Switzerland). We initially isolated 384 single-cell clones from the blasticidin-selected bulk keratinocyte population that had been treated with Cas9n/MC-DP (MC donor plasmid) and sgRNA1 and sgRNA2. Of these, only 17 clonal lines could be expanded up to T75 flask format for protein expression studies.

T7EI Assay

Mismatches upon Cas9/sgRNA-mediated DSB induction and subsequent NHEJ at the desired genomic locus in HEK293AD cells were evaluated via T7EI assays (New England Biolabs, Frankfurt, Germany) on genomic DNA using a *KRT14* exon-6-specific forward primer (5′-CAGGAGATGATTGGCAGCGTGG-3′) and a *KRT14* intron-7-specific reverse primer (5′-AAGCAAGAGGTGGGGGC TGCC-3′) for the PCR. *TACC3* off-target region for sgRNA1 was amplified using a *TACC3* intron-10-specific forward primer (5′-GTGCAGACAGGGTGGTTCCG-3′) and a *TACC3* intron-10-specific reverse primer (5′-TCCCGGTCACCTGCTCTGAC-3′). The digest was performed according to the manufacturer's protocol.

Integration and HDR Efficiency Analysis

For analysis of site-specific integration and recombination, genomic DNA of pre-selected Cas9n/MC-DP and sgRNA1- and sgRNA2-treated keratinocytes was used. The target region for site-specific integration was PCR-amplified using a forward primer (5′-GATGGTAA GACCCTGCTAGCGAATTCCCT-3′) binding to the multiple cloning site of the MC-DP and a reverse primer (5′-GATGCTTCTCC CACTTTCTCCCC-3′) binding to the endogenous 3′ downstream sequence of the *KRT14* gene. For estimation of the HDR efficiency, we PCR-amplified the *KRT14* target region using a forward primer binding to *KRT14* exon 6 (5′-CAGGAGATGATTGGCAGCG TGG-3′) and again a reverse primer binding to the endogenous 3′ downstream sequence (5′-GATGCTTCTCCCACTTTCTCCCC-3′) of the *KRT14* gene, resulting in a PCR product of 1,189 bp, which was subsequently digested with EcoRI restriction enzyme (Thermo Fisher). To minimize the size of the PCR product and facilitate subcloning, we performed a nested PCR using a forward primer binding to exon 6 (5′-CAGGAGATGATTGGCAGCGTGG-3′) and a reverse primer binding to intron 7 (5′-AAGCAAGAGGTGGGGGCT GCC-3′). For subcloning of the PCR product, the StrataClone PCR Cloning Kit (Aligent Technologies, Santa Clara, CA, USA) was used according to the manufacturer's protocol. Single clones were analyzed via EcoRI digestion and Sanger sequencing.

Semiquantitative Real-Time PCR

Total RNA was isolated from cultured keratinocytes using an innuPREP RNA Mini Kit (Analytik Jena, Jena, Germany). cDNA was synthesized from 2 μg of total RNA, using iScript cDNA Synthesis Kit (Bio-Rad). 100 ng of cDNA and 15 pmol of each primer were added to each reaction. Reactions were prepared as master mixes, and two reactions were analyzed per sample. Semi-quantitative real-time PCR was performed to analyze mRNA expression levels of *KRT14*. For amplification of the transcripts, the following primers were used: keratin-14: *KRT14*_fw: 5′-GAGGATATGGTGGTGGCCTTG GTGCTGG-3′ and *KRT14*_rv: 5′- GATCGGATCCTTGGTGCGGA AGTCATCCG-3′. PCR conditions were 3 min at 95°C followed by 50 cycles of 30 s at 95°C, 30 s at 64°C, and 30 s at 72°C. Semi-quantitative real-time PCR was performed using the Bio-Rad iCycler System and Bio-Rad iQ SYBR Green Supermix Kit (Bio-Rad). At least 9 different runs with duplicates were analyzed using 3 different RNA samples of each cell line. Statistics were performed using the one-way ANOVA-Tukey's multiple comparison test. Transcript levels were calculated after normalization to glyceraldehyde 3-phosphate dehydrogenase (GAPDH; *GAPDH*_fw: 5′- GCCAACGTGTCAGTGGT GGA-3′; *GAPDH*_rv: 5′- CACCACCCTGTTGCTGTAGCC-3′).

To analyze correction of the mutation and accurate integration of the MC sequence at RNA level, we used a forward primer binding to the exon 5-exon 6 junction (5′-AGCTCAGCATGAAAGCATCCCT-3′) and a reverse primer binding to exon 8 (5′-CATCGTGCACATCC ATGACCTTGGTG-3′) of *KRT14*. The resulting PCR fragment was confirmed by sequence analysis.

Protein Isolation and Western Blot Analysis

2.5×10^5 EBS keratinocytes were cultivated in keratinocyte SFM GIBCO (Invitrogen, Paisley, UK) and grown to 70%–80% confluence. Whole cell lysates were generated by lysing the cell pellet in radioimmunoprecipitation assay (RIPA) buffer (Santa Cruz Biotechnology, Heidelberg, Germany). Whole cell lysates were centrifuged at full speed at 4°C for 20 min, and supernatant was frozen at −20°C until usage.

Protein samples were denatured for 5 min at 95°C in 4× loading buffer (0.25 M Tris-HCl; 8% SDS; 30% glycerol; 0.02% bromphenol blue; 0.3 M β-mercaptoethanol [pH 6.8]). The procedure of western blotting was performed as previously described.[40,41] Ponceau red (Sigma-Aldrich, St. Louis, MO, USA) staining of the nitrocellulose membrane was performed after electro-blotting. Nitrocellulose membrane was blocked with blocking reagent (Roche Diagnostics, Mannheim, Germany) diluted 1:10 in Tris-buffered saline with 0.2% Tween (TBS-T) for 1 hr at room temperature (RT). For detection of K14, a mouse anti-cytokeratin 14 antibody (LL001:sc53253) (Santa Cruz Biotechnology, Heidelberg, Germany) diluted 1:400 in TBS-T and blocking reagent was used and incubated at 4°C overnight. A polyclonal α-actinin antibody (H-300:sc15335) served as loading control, diluted 1:1,000 in TBS-T and blocking reagent. As secondary antibodies, either the horseradish peroxidase (HRP) Envision+-labeled anti-mouse or anti-rabbit antibody (Dako, Santa Clara, CA, USA) diluted 1:200 in TBS-T was used. Nitrocellulose membrane was incubated for 1 hr at RT. Protein bands were visualized using the Immobilon Western Chemiluminescent HRP Substrate (Merck, Darmstadt, Germany) and the ChemiDoc XRS Imager (Bio-Rad, Hercules, CA, USA).

Immunofluorescence Staining of Cytokeratin 14 after Heat Shock

2.5×10^5 keratinocytes were seeded into 35 mm glass-bottom dishes (MatTek In Vitro Life Science Laboratories, Bratislava, Slovak Republic) and grown to 50%–70% confluency. Heat shock was performed in a water bath at 43°C for 30 min, followed by a 15 min recovery time at 37°C and 5% CO_2 in a humidified incubator. Cells were fixed with 4% formaldehyde solution (Sigma-Aldrich) overnight at RT. The next day cells were treated with an antigen retrieval buffer (1 mM EDTA and 0.05% Tween in PBS [pH 8]) at 95°C for 40 min in a water bath. Permeabilization and staining of the cells were performed in a

single step. The mouse anti-cytokeratin 14 antibody (LL001:sc53253) was used in a 1:100 dilution, diluted in 0.3% Triton X, blocking reagent (1:10), and TBS-T. As secondary antibody, either Alexa Fluor 488 goat anti-mouse IgG (Invitrogen, Paisley, UK) (1:400 in TBS-T) or Alexa Fluor 594 goat anti-mouse IgG (Invitrogen, Paisley, UK) (1:400 in TBS-T) was used for 1 hr at RT. DAPI was diluted 1:4,000 in TBS-T and added to the cells for 10 min. Cells were analyzed using an inverted microscope system, which includes the laser scanning confocal microscope Zeiss LSM 700 and the Axio Observer Z1 (Carl Zeiss, Oberkochen, Germany).

Off-Target Prediction

Off-target prediction was performed using the BLASTn (https://blast.ncbi.nlm.nih.gov/Blast.cgi). Both sgRNAs were compared with the genomic and transcript databases to identify potential off-target loci.

NGS

We designed a comprehensive AmpliSeq panel to perform NGS analyses on the Ion Torrent Personal Genome Machine (PGM) platform. A setup of a 400 bp customized panel was chosen to cover the cutting sites of the single gRNA constructs within the on-target region of the *KRT14* gene, as well as cutting sites within predicted off-target regions; primers are listed in Table S2. A mean vertical coverage of at least 5,000 reads was planned. The library preparation, template preparation, and the sequencing run were performed according to manufacturer's protocols (Thermo Fisher Scientific/Life Technologies, Carlsbad, CA, USA). Data analysis was implemented on the Integrative Genome Viewer (IGV). We attained a mean coverage of about 4,072 reads for the EBS cell line and about 1,602 reads for HEK293 cells with our customized panel.

SUPPLEMENTAL INFORMATION

Supplemental Information includes three figures and two tables and can be found with this article online at http://dx.doi.org/10.1016/j.ymthe.2017.08.015.

AUTHOR CONTRIBUTIONS

Conceptualization, T.K. and U.K.; Methodology, T.K., U.K., J.P.H., and E.M.M.; Investigation, T.K., S.H., P.P., T.L., and M.A.; Validation, A.K.; Writing – Original Draft, T.K., P.P., and U.K.; Writing – Review & Editing, J.R., J.W.B., and J.P.H.; Resources, V.W., A.K., and M.A.; Supervision, U.K., E.M.M., and J.R.

ACKNOWLEDGMENTS

The authors thank Franz Zimmermann for his suggestions and critical scientific input. Special thanks to Univ.-Prof. Dr. Eva Rohde and Karin Roider, MSc, of the Spinal Cord Injury and Tissue Regeneration Center Salzburg (SCI-TReCS) for providing their Core Facility for Microscopy. This work was supported by DEBRA Austria.

REFERENCES

1. Jinek, M., Chylinski, K., Fonfara, I., Hauer, M., Doudna, J.A., and Charpentier, E. (2012). A programmable dual-RNA-guided DNA endonuclease in adaptive bacterial immunity. Science *337*, 816–821.
2. March, O.P., Reichelt, J., and Koller, U. (2017). Gene editing for skin diseases: designer nucleases as tools for gene therapy of skin fragility disorders. Exp. Physiol., Published online March 17, 2017. http://dx.doi.org/10.1113/EP086044.
3. Aushev, M., Koller, U., Mussolino, C., Cathomen, T., and Reichelt, J. (2017). Traceless targeting and isolation of gene-edited immortalized keratinocytes from epidermolysis bullosa simplex patients. Mol. Ther. Methods Clin. Dev. *6*, 112–123.
4. Hainzl, S., Peking, P., Kocher, T., Murauer, E.M., Larcher, F., Del Rio, M., Duarte, B., Steiner, M., Klausegger, A., Bauer, J.W., et al. (2017). COL7A1 editing via CRISPR/Cas9 in recessive dystrophic epidermolysis bullosa. Mol. Ther., Published online July 13, 2017. http://dx.doi.org/10.1016/j.ymthe.2017.07.005.
5. Ran, F.A., Hsu, P.D., Lin, C.Y., Gootenberg, J.S., Konermann, S., Trevino, A.E., Scott, D.A., Inoue, A., Matoba, S., Zhang, Y., and Zhang, F. (2013). Double nicking by RNA-guided CRISPR Cas9 for enhanced genome editing specificity. Cell *154*, 1380–1389.
6. Ran, F.A., Hsu, P.D., Wright, J., Agarwala, V., Scott, D.A., and Zhang, F. (2013). Genome engineering using the CRISPR-Cas9 system. Nat. Protoc. *8*, 2281–2308.
7. Dianov, G.L., and Hübscher, U. (2013). Mammalian base excision repair: the forgotten archangel. Nucleic Acids Res. *41*, 3483–3490.
8. Horn, H.M., and Tidman, M.J. (2000). The clinical spectrum of epidermolysis bullosa simplex. Br. J. Dermatol. *142*, 468–472.
9. Fine, J.D., Bruckner-Tuderman, L., Eady, R.A., Bauer, E.A., Bauer, J.W., Has, C., Heagerty, A., Hintner, H., Hovnanian, A., Jonkman, M.F., et al. (2014). Inherited epidermolysis bullosa: updated recommendations on diagnosis and classification. J. Am. Acad. Dermatol. *70*, 1103–1126.
10. Coulombe, P.A., Kerns, M.L., and Fuchs, E. (2009). Epidermolysis bullosa simplex: a paradigm for disorders of tissue fragility. J. Clin. Invest. *119*, 1784–1793.
11. Szeverenyi, I., Cassidy, A.J., Chung, C.W., Lee, B.T., Common, J.E., Ogg, S.C., Chen, H., Sim, S.Y., Goh, W.L., Ng, K.W., et al. (2008). The Human Intermediate Filament Database: comprehensive information on a gene family involved in many human diseases. Hum. Mutat. *29*, 351–360.
12. Wu, Z., and Feng, G. (2015). Progress of application and off-target effects of CRISPR/Cas9. Yi Chuan *37*, 1003–1010.
13. Fu, Y., Foden, J.A., Khayter, C., Maeder, M.L., Reyon, D., Joung, J.K., and Sander, J.D. (2013). High-frequency off-target mutagenesis induced by CRISPR-Cas nucleases in human cells. Nat. Biotechnol. *31*, 822–826.
14. Cong, L., Ran, F.A., Cox, D., Lin, S., Barretto, R., Habib, N., Hsu, P.D., Wu, X., Jiang, W., Marraffini, L.A., and Zhang, F. (2013). Multiplex genome engineering using CRISPR/Cas systems. Science *339*, 819–823.
15. Wally, V., Lettner, T., Peking, P., Peckl-Schmid, D., Murauer, E.M., Hainzl, S., Hintner, H., and Bauer, J.W. (2013). The pathogenetic role of IL-1β in severe epidermolysis bullosa simplex. J. Invest. Dermatol. *133*, 1901–1903.
16. Glász-Bóna, A., Medvecz, M., Sajó, R., Lepesi-Benko, R., Tulassay, Z., Katona, M., Hatvani, Z., Blazsek, A., and Kárpáti, S. (2009). Easy method for keratin 14 gene amplification to exclude pseudogene sequences: new keratin 5 and 14 mutations in epidermolysis bullosa simplex. J. Invest. Dermatol. *129*, 229–231.
17. Kaneko, S., Hamada, T., Kawano, Y., Hashimoto, T., and Morita, E. (2011). Missense mutation at the helix termination region in the 2B domain of keratin 14 in a Japanese family with epidermolysis bullosa simplex, generalized, other. Int. J. Dermatol. *50*, 436–438.
18. Montague, T.G., Cruz, J.M., Gagnon, J.A., Church, G.M., and Valen, E. (2014). CHOPCHOP: a CRISPR/Cas9 and TALEN web tool for genome editing. Nucleic Acids Res. *42* (Web Server issue), W401–W407.
19. Bloom, K., Ely, A., and Arbuthnot, P. (2017). A T7 endonuclease I assay to detect Talen-mediated targeted mutation of HBV cccDNA. Methods Mol. Biol. *1540*, 85–95.
20. Guschin, D.Y., Waite, A.J., Katibah, G.E., Miller, J.C., Holmes, M.C., and Rebar, E.J. (2010). A rapid and general assay for monitoring endogenous gene modification. Methods Mol. Biol. *649*, 247–256.
21. Corpet, F. (1988). Multiple sequence alignment with hierarchical clustering. Nucleic Acids Res. *16*, 10881–10890.
22. Wally, V., Brunner, M., Lettner, T., Wagner, M., Koller, U., Trost, A., Murauer, E.M., Hainzl, S., Hintner, H., and Bauer, J.W. (2010). K14 mRNA reprogramming for dominant epidermolysis bullosa simplex. Hum. Mol. Genet. *19*, 4715–4725.

23. Abitbol, R.J., and Zhou, L.H. (2009). Treatment of epidermolysis bullosa simplex, Weber-Cockayne type, with botulinum toxin type A. Arch. Dermatol. *145*, 13–15.

24. Neufeld-Kaiser, W., and Sybert, V.P. (1997). Is cyproheptadine effective in the treatment of subjects with epidermolysis bullosa simplex-Dowling-Meara? Arch. Dermatol. *133*, 251–252.

25. Veien, N.K., and Buus, S.K. (2000). Treatment of epidermolysis bullosa simplex (EBS) with tetracycline. Arch. Dermatol. *136*, 424–425.

26. Chiaverini, C., Fontas, E., Vabres, P., Bessis, D., Mazereeuw, J., Charlesworth, A., Meneguzzi, G., and Lacour, J.P. (2015). Oral erythromycin therapy in epidermolysis bullosa simplex generalized severe. Br. J. Dermatol. *173*, 563–564.

27. Retief, C.R., Malkinson, F.D., and Pearson, R.W. (1999). Two familial cases of epidermolysis bullosa simplex successfully treated with tetracycline. Arch. Dermatol. *135*, 997–998.

28. Kerns, M.L., Guss, L., Fahey, J., Cohen, B., Hakim, J.M., Sung, S., Lu, R.G., and Coulombe, P.A. (2017). Randomized, split-body, single-blinded clinical trial of topical broccoli sprout extract: assessing the feasibility of its use in keratin-based disorders. J. Am. Acad. Dermatol. *76*, 449–453.e1.

29. Wally, V., Kitzmueller, S., Lagler, F., Moder, A., Hitzl, W., Wolkersdorfer, M., Hofbauer, P., Felder, T.K., Dornauer, M., Diem, A., et al. (2013). Topical diacerein for epidermolysis bullosa: a randomized controlled pilot study. Orphanet J. Rare Dis. *8*, 69.

30. Bauer, J.W., Koller, J., Murauer, E.M., De Rosa, L., Enzo, E., Carulli, S., Bondanza, S., Recchia, A., Muss, W., Diem, A., et al. (2017). Closure of a large chronic wound through transplantation of gene-corrected epidermal stem cells. J. Invest. Dermatol. *137*, 778–781.

31. Mavilio, F., Pellegrini, G., Ferrari, S., Di Nunzio, F., Di Iorio, E., Recchia, A., Maruggi, G., Ferrari, G., Provasi, E., Bonini, C., et al. (2006). Correction of junctional epidermolysis bullosa by transplantation of genetically modified epidermal stem cells. Nat. Med. *12*, 1397–1402.

32. Siprashvili, Z., Nguyen, N.T., Gorell, E.S., Loutit, K., Khuu, P., Furukawa, L.K., Lorenz, H.P., Leung, T.H., Keene, D.R., Rieger, K.E., et al. (2016). Safety and wound outcomes following genetically corrected autologous epidermal grafts in patients with recessive dystrophic epidermolysis bullosa. JAMA *316*, 1808–1817.

33. Cao, T., Longley, M.A., Wang, X.J., and Roop, D.R. (2001). An inducible mouse model for epidermolysis bullosa simplex: implications for gene therapy. J. Cell Biol. *152*, 651–656.

34. Chamcheu, J.C., Navsaria, H., Pihl-Lundin, I., Liovic, M., Vahlquist, A., and Törmä, H. (2011). Chemical chaperones protect epidermolysis bullosa simplex keratinocytes from heat stress-induced keratin aggregation: involvement of heat shock proteins and MAP kinases. J. Invest. Dermatol. *131*, 1684–1691.

35. Werner, N.S., Windoffer, R., Strnad, P., Grund, C., Leube, R.E., and Magin, T.M. (2004). Epidermolysis bullosa simplex-type mutations alter the dynamics of the keratin cytoskeleton and reveal a contribution of actin to the transport of keratin subunits. Mol. Biol. Cell *15*, 990–1002.

36. Petek, L.M., Fleckman, P., and Miller, D.G. (2010). Efficient KRT14 targeting and functional characterization of transplanted human keratinocytes for the treatment of epidermolysis bullosa simplex. Mol. Ther. *18*, 1624–1632.

37. Smith, C., Gore, A., Yan, W., Abalde-Atristain, L., Li, Z., He, C., Wang, Y., Brodsky, R.A., Zhang, K., Cheng, L., and Ye, Z. (2014). Whole-genome sequencing analysis reveals high specificity of CRISPR/Cas9 and TALEN-based genome editing in human iPSCs. Cell Stem Cell *15*, 12–13.

38. Duarte, B., Miselli, F., Murillas, R., Espinosa-Hevia, L., Cigudosa, J.C., Recchia, A., Del Río, M., and Larcher, F. (2014). Long-term skin regeneration from a gene-targeted human epidermal stem cell clone. Mol. Ther. *22*, 1878–1880.

39. Larcher, F., Dellambra, E., Rico, L., Bondanza, S., Murillas, R., Cattoglio, C., Mavilio, F., Jorcano, J.L., Zambruno, G., and Del Rio, M. (2007). Long-term engraftment of single genetically modified human epidermal holoclones enables safety pre-assessment of cutaneous gene therapy. Mol. Ther. *15*, 1670–1676.

40. Peking, P., Koller, U., Hainzl, S., Kitzmueller, S., Kocher, T., Mayr, E., Nyström, A., Lener, T., Reichelt, J., Bauer, J.W., and Murauer, E.M. (2016). A gene gun-mediated nonviral RNA trans-splicing strategy for Col7a1 repair. Mol. Ther. Nucleic Acids *5*, e287.

41. Tockner, B., Kocher, T., Hainzl, S., Reichelt, J., Bauer, J.W., Koller, U., and Murauer, E.M. (2016). Construction and validation of an RNA trans-splicing molecule suitable to repair a large number of COL7A1 mutations. Gene Ther. *23*, 775–784.

YMTHE, Volume *25*

Supplemental Information

Cut and Paste: Efficient Homology-Directed Repair of a Dominant Negative *KRT14* Mutation via CRISPR/Cas9 Nickases

Thomas Kocher, Patricia Peking, Alfred Klausegger, Eva Maria Murauer, Josefina Piñón Hofbauer, Verena Wally, Thomas Lettner, Stefan Hainzl, Michael Ablinger, Johann Wolfgang Bauer, Julia Reichelt, and Ulrich Koller

Supplementary Data

HEK 293

sgRNA 1	3´ggaggagacgtccggacccg 5´						
localization	target sequence	Cas9n/sgRNA1+2			spCas9/sgRNA1		
on-target sgRNA1	on-target sgRNA1	PAM+2	PAM+3	PAM+4	PAM+2	PAM+3	PAM+4
Chr. 17 (41583086 to 41583064) *KRT14* Intron 7 (sense)	5´cctcctcctctgcaggcctgggc 3´	0,31	0,31	0,24	3,38	6,56	16,10
off-targets sgRNA1	off-targets sgRNA1	PAM+/- 2	PAM+/- 3	PAM+/- 4	PAM+/- 2	PAM+/- 3	PAM+/- 4
Chr. 4 (1738178 to 1738200) *TACC3* Intron 10 (sense)	5´ccccctcctctgcaggcctgggc 3´	0,00	0,00	0,00	0,00	0,00	4,37
Chr. 21 (26917895 to 26917917) *APP* Intron 7 (antisense)	3´ctacataattcgtctcctcctcc 5´	0,35	0,17	0,00	0,23	0,05	0,00
Chr. 21 (44907189 to 44907211) *ITGB2* Intron 4 (antisense)	3´ttaaggtccgcgtctcctcctcc 5´	0,15	0,37	0,37	0,00	0,00	0,00
Chr. 17 (2787805 to 2787827) *RAP1GAP2* Intron 2 (sense)	5´cctcctcctctgctggccttccac 3´	0,00	0,00	0,16	0,00	0,00	2,50
Chr. 21 (42294475 to 42294497) *ABCG1* Intron 14 (sense)	5´gagcctcctctgcaggaggccag 3´	0,00	0,00	0,00	0,00	0,00	0,00
Chr. 21 (44724272 to 44724294) *PDXK* Intron 4 (sense)	5´cttcctcctctgcacgcctccgt 3´	0,08	0,00	0,00	0,87	0,00	0,00
Chr. 21 (40725550 to 40725572) *IGSF5* Intron 7 (sense)	5´actcctcctctgcaggatgaaca 3´	0,00	0,00	0,07	0,13	0,06	0,00
Chr. 21 (36962293 to 36962315) *HLCS* Intron 1 (antisense)	3´gatgctcctctgcaggccgcagg 5´	0,30	0,00	0,00	0,47	0,00	0,00
sgRNA 2	5´agcaggtctaggcattggct 3´						
localization	target sequence	Cas9n/sgRNA1+2			spCas9/sgRNA2		
on-target sgRNA2	on-target sgRNA2	PAM-2	PAM-3	PAM-4	PAM-2	PAM-3	PAM-4
Chr. 17 (41583040 to 41583018) *KRT14* Intron 7 (antisense)	3´tcgtccagatccgtaaccgatcc 5´	0,00	0,00	0,00	0,00	1,84	28,65
off-targets sgRNA2	off-targets sgRNA2	PAM+/- 2	PAM+/- 3	PAM+/- 4	PAM+/- 2	PAM+/- 3	PAM+/- 4
Chr. 11 (2936955 to 2936977) *SLC22A18* Intron 6 (antisense)	3´ccgttaccttccgtaaccgatcc 5´	0,00	0,00	0,00	0,00	0,00	0,00
Chr. 4 (67871082 to 67871104) *TMPRSS11D* Intron 1 (sense)	5´cctagccaatgccttcctaggaa 3´	0,00	0,00	0,00	0,20	0,09	0,43
Chr. 4 (113999328 to 113999350) *ANK2* Intron 1 (antisense)	3´cttaataaacccgtaaccgatcc 5´	0,00	0,00	0,00	0,28	0,23	0,00
Chr. 11 (52028437 to 52028459) *AAMDC* Intron 3 (antisense)	3´acccaatatccgtaaccgattt 5´	0,00	0,00	0,00	0,03	0,00	0,00
Chr. 5 (36657983 to 36658005) *SLC1A3* Intron 3 (antisense)	3´acttagatatccgtaaccgatta 5´	0,12	0,04	0,00	0,00	0,03	0,00

Supplementary Table 1: DNA cleavage activity of the respective nucleases at potential off-target regions for sgRNA1 and sgRNA2. DNA cleavage activities of sgRNAs at on-target and off-target regions are represented as % indels relative to untreated control. The cut-off for cleavage activity was set to 0.5%. Colored boxes indicate cleavage activity of the respective Cas9/sgRNA at on-target and off-target regions. On-target and off-target region sequences are listed, with red letters indicating the PAM position, blue letters indicating mismatches between the sgRNA on-target binding sites and the potential off-target regions and black letters indicating matches between on-target and off-target regions.

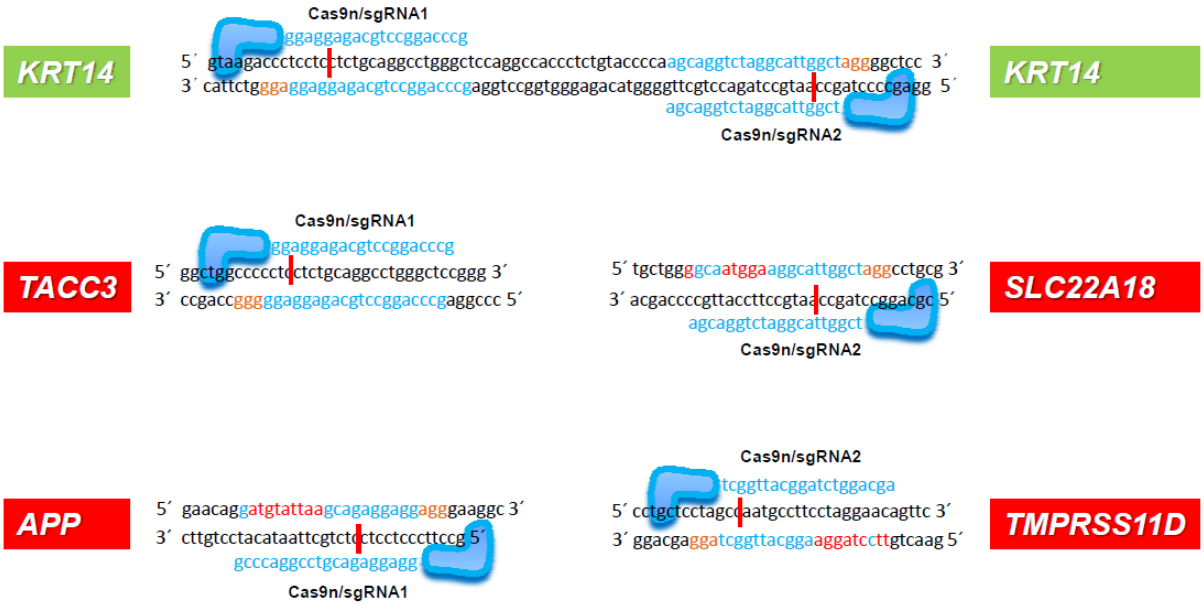

Supplementary Figure 1: Schematic depiction of on-target and off-target cutting sites. DNA cleavage sites of the two sgRNAs at on-target and predicted off-target regions are shown, with orange letters indicating the PAM position, red letters indicating mismatches between the sgRNA on-target binding sites and the potential off-target regions and blue letters indicating matches between on-target and off-target regions. Two predicted off-targets are depicted for each sgRNA, showing either antisense strand or sense strand targeting.

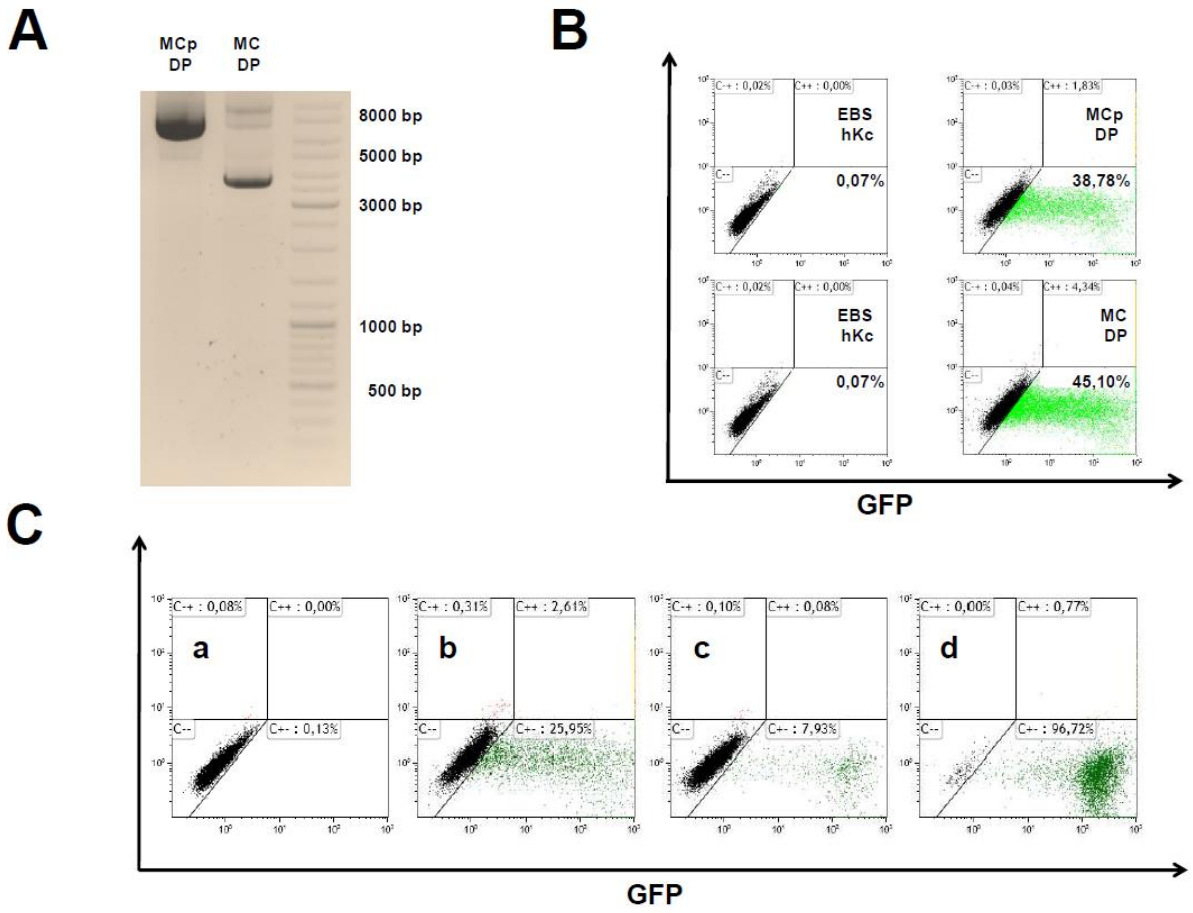

Supplementary Figure 2: Transfection efficiency and selection efficiency using a MC donor plasmid. (A) Size comparison of the parental MC donor plasmid (MCp-DP) and the MC donor plasmid. **(B)** Flow cytometric analysis of EBS-gen sev keratinocytes 48 hours post transfection revealed differences in transfection efficiencies. **(C)** Selection and sorting strategy for the different CRISPR/Cas9 gene editing approaches. Representative FACS blots show (a) untreated patient cells, treated cells (b) after transfection with the MC DP, (c) after blasticidin selection start and (d) after blasticidin selection stop.

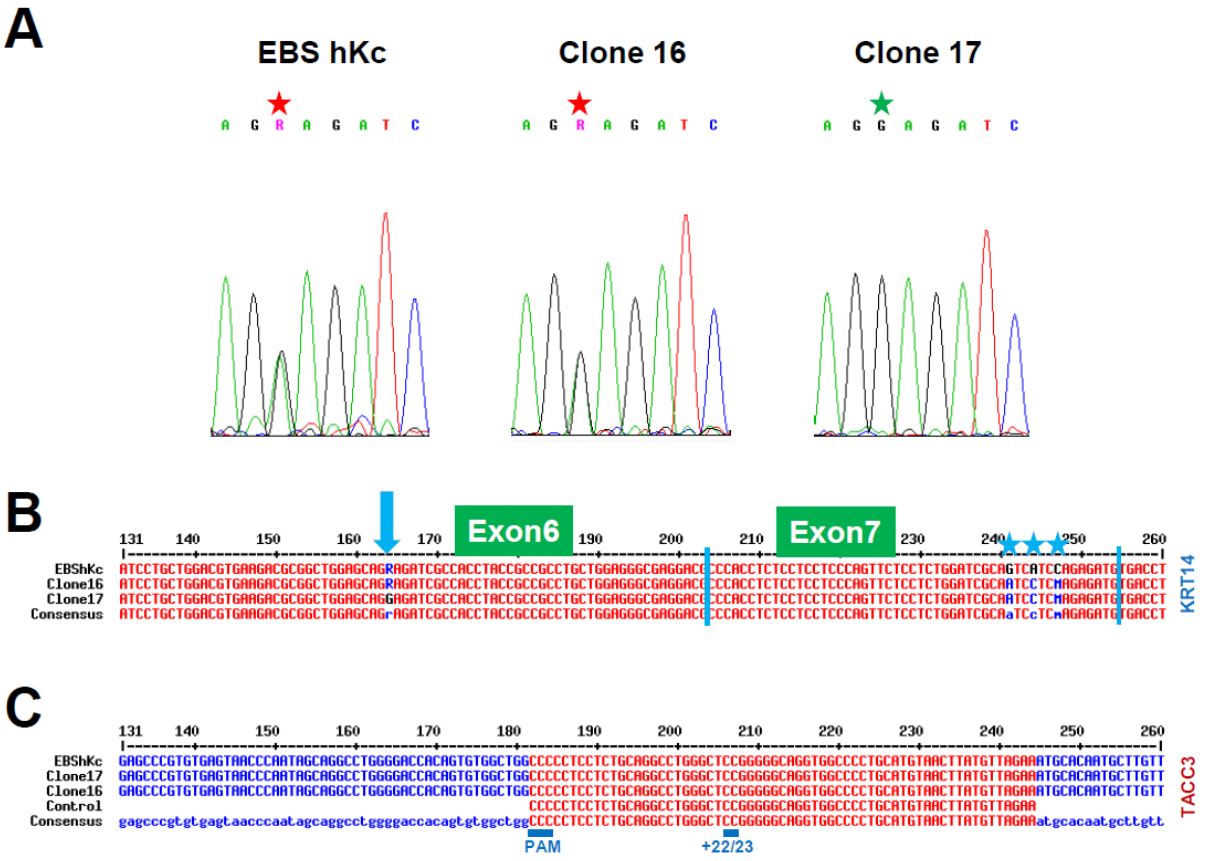

Supplementary Figure 3: Correction of the dominantly inherited missense mutation (c.1231G>A) within exon 6 of *KRT14* gene in single cell clones. (A) Amplification of endogenous *KRT14* using a forward primer binding to exon 3 and a reverse primer binding exon 7 and the integrated restriction sites (EcoRI and NheI sequence). Correction of the mutation within exon 6 of *KRT14* was confirmed by sequence analysis of the PCR product. Red star: heterozygous mutation (A>G) within exon 6; green star: repaired mutation (A>G) within exon 6 of targeted allele. **(B)** Amplification of expressed *KRT14* (cDNA) using a forward primer binding to the exon 5/exon 6 junction and a reverse primer binding to exon 8. Correction of the mutation and accurate integration of the MC sequence was confirmed by sequence analysis of the PCR product. Blue arrow: position of the mutation (position 164); R indicates the heterozygous mutation. G indicates correction of the mutation. blue stars: silent mutations. **(C)** Sequence analysis of the predicted off-target region intron 10 of *TACC3*. The predicted off-target region for sgRNA1 was PCR-amplified using a primer pair binding specifically within *TACC3* intron 10. Genomic DNA isolated from single cell clones treated with Cas9n-sgRNA1+2/ MC–DP and untreated EBS keratinocytes was used as PCR template. PAM +22/23 represents positions of typical on-target indel formations within intron 7 of *KRT14* via double nicking. Sequence alignment was performed with the software "Multiple sequence alignment with hierarchical clustering" (21).

localization	HEK293 (mean coverage; reads)	EBS hKc (mean coverage; reads)	forward primer	reverse primer
on-target	**on-target**	**on-target**	**on-target**	**on-target**
KRT14 **Intron 7**	**1847**	**10075**	5´- ACCATGTATCTAATGATCCTGTCCTTTTCTA -3´	5´- CTCAGCCCCTCACGGAG -3´
off-targets sgRNA1	**off-targets sgRNA1**	**off-targets sgRNA1**	**off-targets sgRNA1**	**off-targets sgRNA1**
TACC3 **Intron 10**	**2043**	**6629**	5´- CCAACATCCACACCAGTGTTGT -3´	5´- GGCACCCTTTCTGCAGAAAGTA -3´
APP **Intron 7**	**1041**	**4549**	5´- GGAAGGAAGGAAGGAAAGAGTCATG -3´	5´- GCACTCTTCTACCAAAACATTTTCAGT -3´
ITGB2 **Intron 4**	**462**	**2172**	5´- CCATTGTGGTCTTCCTGGGTTT -3´	5´- CTAGAGGCAGAGGAGGAGGCGATA -3´
RAP1GAP2 **Intron 2**	**1312**	**4335**	5´- GCTCATGTAGCAAGTGGCTTCA -3´	5´- GGGAAGGCTACAGGAAGGATGA -3´
ABCG1 **Intron 14**	**450**	**1638**	5´- GCAGACGGCAGTCTGTTGAG -3´	5´- GAAAGTGGCCACCTGGAGTT -3´
PDXK **Intron 4**	**954**	**2827**	5´- CCCTAAAGGTTATACGAGGGACAAGT -3´	5´- CCACTATACGAGCACACTGACA -3´
IGSF5 **Intron 7**	**1367**	**4819**	5´- GGAATGCTGGAAAACTAGACCTACT -3´	5´- ATGCAATCTGGAATACACATGGGA -3´
HLCS **Intron 1**	**599**	**2273**	5´- GTTCTGCTTCAAGTATAAAAGGAGACACA -3´	5´- CCGGTTAGCTACTGTGTGCTAA -3´
off-targets sgRNA2	**off-targets sgRNA2**	**off-targets sgRNA2**	**off-targets sgRNA2**	**off-targets sgRNA2**
SLC22A18 **Intron 6**	**2711**	**2053**	5´- GTCCTCAGCTTCACCTGCAT -3´	5´- CACTTGGCTTCTATGATGTCAGCA -3´
TMPRSS11D **Intron 1**	**2084**	**4277**	5´- TTATCTGTCTCCCTCCACCAGTT -3´	5´- TGAAAGGGAAACACTTTGAGTTTCTTTAAA -3´
ANK2 **Intron 1**	**1111**	**2550**	5´- AAGTACACATGCAAGCCCTGAA -3´	5´- TCCCTGAGTCTTATAAATTTTTCCACCAAA -3´
AAMDC **Intron 3**	**2477**	**2962**	5´- CCGGCTATCCTCCAAATTCTTAACA -3´	5´- TGTTACCTGGATGTGAGACATGGA -3´
SLC1A3 **Intron 3**	**3972**	**5858**	5´- GCTACCAGTTGCAGCATTGACT -3´	5´- GTGAGAATGCCATCATTTGACCAAG -3´

Supplementary Table 2: NGS primer combinations and mean coverage of the designed panel.